The Thesis Committee for Mayowa Olugbenga Oyedere
Certifies that this is the approved version of the following thesis:

Lost Circulation Mitigation in Low Permeability Formations using Fluid Additives that Encourage Fracture Termination against Pre-existing Fractures

APPROVED BY
SUPERVISING COMMITTEE:

Supervisor:

Ken Gray

Co - supervisor:

Mark W. McClure

Lost Circulation Mitigation in Low Permeability Formations using Fluid Additives that Encourage Fracture Termination against Pre-existing Fractures

by

Mayowa Olugbenga Oyedere, B, S.

Thesis

Presented to the Faculty of the Graduate School of

The University of Texas at Austin

in Partial Fulfillment

of the Requirements

for the Degree of

Master of Science in Engineering

The University of Texas at Austin

December 2015

Dedication

This thesis is dedicated to the One who is beyond comprehension; the very essence of my existence; The Almighty God.

Acknowledgements

I would like thank my advisor Dr. Mark M. McClure for giving me the opportunity to pursue my Master's degree under his supervision; it has truly been a great experience working with him. I have had the privilege of sharing ideas and learning a great deal from his knowledge and experience. His constant support, insightful feedback and reviews helped in the successful completion of this work.

Special thanks to Dr. Ken Gray for his contribution to this work. Comments and recommendations from his years of experience constantly helped proffer solutions to problems that arose. My appreciation also goes to the Wider Windows JIP sponsors for providing the financial support to successfully complete this work and my degree program.

I would like to thank TACC for providing the platform to run all the simulations and resolving issues promptly.

Finally, I would like to thank my family for their unending love, support and prayers throughout my degree program. Words are not enough to express my gratitude. To all my amazing friends, "You guys are the best".

Abstract

Lost Circulation Mitigation in Low Permeability Formations using Fluid Additives that Encourage Fracture Termination against Pre-existing Fractures

Mayowa Olugbenga Oyedere, M.S.E.

The University of Texas at Austin, 2015

Supervisor: Ken Gray

Co-Supervisor: Mark W. McClure

Lost circulation is a long-standing challenge in the petroleum industry and a major contributor to non-productive rig time during drilling. Over the years, the industry has developed various lost circulation mitigation (LCM) techniques, several of which have yielded positive results. Lost circulation remains a particular problem in formations that have very low permeability but which do not have high clay content.

Low permeability formations, especially shales, often contain natural fractures. When a hydraulic fracture is induced during drilling, it may interact with these pre-existing fractures and other planes of weakness by either terminating or crossing. We investigated whether these interactions could be exploited to mitigate lost circulation.

A novel hypothesis for how low matrix permeability could encourage termination through a time-dependent poroelastic effect was developed and tested using a hydraulic

fracturing simulator (CFRAC). Previous studies have shown that crossing occurs when hydraulic fractures are able to reinitiate on the other side of the plane of weakness. A sensitivity study was performed to investigate the effect of permeability, tensile yield strength, and the rate of hydraulic fracture propagation on the ability for incipient fractures to initiate on the opposite side of the preexisting fracture. Results showed that in low permeability formations, a high rate of hydraulic fracture propagation may cause termination. Based on the hypothesis and the results of the sensitivity study, a semi-analytical time-dependent model to predict crossing was developed and implemented into CFRAC. CFRAC's ability to simulate the injection of fluids with different injection rates and fluid viscosities was used to design a two-step LCM pumping sequence of high injection rate and low fluid viscosity, followed by lower injection rate and high fluid viscosity.

Table of Contents

List of Tables

List of Figures

Chapter 1 : Introduction

Lost circulation is the partial or complete loss of drilling fluid to the formation when drilling, circulating fluid, or running casing (Chilingarian and Vorabutr, 1983). Most lost circulation events occur when drilling is performed in an overbalanced state- where the equivalent circulation density (ECD) of the mud in the wellbore exceeds the fracture gradient. This creates fractures through which the drilling mud flows and leaks off to the formation. Wells are usually drilled with an overbalanced ECD in order to counteract the pore pressure of the formation and prevent an uncontrolled influx of reservoir fluid into the well- a phenomenon known as a kick and which can eventually lead to a blowout. Overbalanced ECD also prevents borehole stability problems associated with the removal of rock during drilling. The fracture gradient and pore pressure represent the upper and lower limits on ECD and this range is referred to as the mud weight window or the drilling margin. The size of the mud weight window varies during the drilling process. For efficient drilling, the mud weight should be kept within this window at all times.

Lost circulation is one of the most fundamental problems encountered in drilling and is a major contributor to non-productive time (NPT). This has a direct economic impact on the overall cost of drilling because of the rig usage charges. It is estimated that lost circulation problems cost the industry about US$800 million per year (Ivan et al., 2003, Murchison, 2006).

1.1 MOTIVATION

Various techniques that use different mechanisms have been developed over the years in the industry to curb the threat of lost circulation. Howard and Scott (1951) in their analysis of lost circulation control and prevention showed through laboratory test and tests in shallow and stimulated wells that it was possible to greatly minimize lost circulation by effectively plugging up the fractures with a proper range of particle sizes at the instance the fractures are created. In more recent times, lost circulation reduction methods have evolved and are often referred to as "wellbore strengthening" techniques (Wang et al., 2008). There are three major methods used to mitigate lost circulation in the industry. However, there is no consensus on which technique works best. All the methods have an overall effect of strengthening the wellbore by increasing the pressure that the wellbore is able withstand without uncontrolled losses.

"Fracture propagation resistance" is the one the major lost circulation mitigation techniques. The drilling mud is treated with lost circulation materials (LCM) which flow into the incipient or already exiting fractures to plug up the fractures and isolate the fluid tip from the fracture tip. This technique was first introduced in the Drilling Engineering Association (DEA) project carried out in the mid 1980's and early 1990's (Morita et al, 1990) to understand the differences observed in the fracture gradient between oil-based muds (OBM) and water-based muds (WBM). It was found out that the fracture initiation pressure did not differ for the different mud types and formations in intact boreholes. Rather, there were substantial differences in the fracture propagation behavior which was dependent on the fluid type and mixture. A phenomenon known as fracture tip screen out was explained to be responsible for the observed differences. When fracture growth starts, there is a spurt of drilling fluid into the void space of the new fracture. If the drilling fluid is treated with LCM, the fluid flow causes the LCM to

accumulate and create a plug that isolates or screens the fracture tip from the invading hydrostatic mud pressure. Hence the buildup of the plug will vary with different types of fluid. When a fracture grows in WBMs, there is a quick fluid loss into the new opening creating a plug or seal that cuts off fluid communication with the fracture tip. This increases the fracture propagation pressure preventing further fracture propagation. In the event, that the mud pressure becomes high enough to break through the barrier, propagation resumes and new LCM begins to accumulate in the fracture until a new barrier is formed. On the other hand, when a fracture grows in OBMs, there is only limited fluid loss into the new fracture opening and the invert emulsion rapidly creates a filtercake on the internal walls of the fracture but does not prevent the flow the drilling mud to the fracture tip. This encourages further fracture propagation even at a pressure lower than that of WBMs (Van Oort et al., 2009).

Stress caging (Aston et al. 2004) is another wellbore strengthening method used in the industry. The method is based on the idea that the hoop stresses in the near wellbore region can be increased by adding appropriate wellbore strengthening materials (WSM) of suitable sizes to the drilling mud. The wellbore is drilled in an overbalanced state in order to create small fractures into which the WSM treated mud flows. The WSM begins to accumulate and bridge at the fracture mouth close to the wellbore isolating the fluid in the fracture from the fluid in the wellbore. As the fluid in the fracture leaks off into the formation, the fracture begins to close against the bridging particles increasing the hoop stress around the wellbore. As a consequence, a higher wellbore pressure is required for the re-initiation of the fracture and also the formation of new ones.

Another wellbore strengthening method used in the industry is called fracture closure stress (FCS) developed by (Dupriest, 2005). It is similar to the stress cage in the way the WSM is

proposed to plug open fractures and inhibit fracture propagation. However there are some fundamental differences between the two mechanisms. In stress cage, fractures are created and their growth is immediately stopped, while FCS is a high fluid loss procedure for existing fractures. During the squeeze stage, as the WSM laden mud flows into the fractures, there is a rapid fluid loss to the matrix leaving behind an immobile mass of particles (at any point in the fracture) that cuts off fluid interaction between the wellbore and the fracture tip. This inadvertently stops fracture propagation and causes a rise in the wellbore pressure and an increases in the fracture width.

The conventional LCMs have been proven to be highly effective in high permeability formations but have been less effective in low permeability formations such as shale (Dupriest, 2005; Van Oort et al., 2009). The LCM methods rely on the leakoff of considerable amount of fluid to the matrix which does not occur in low permeability formations. The focus of this thesis is on low permeability formations.

1.2 PREMISE

When a propagating hydraulic fracture intersects a natural fracture, there are three possible modes of interaction– opening (dilation), slippage (arrest), and crossing (Chuprakov et al., 2011; Thiercelin, 2009). During the propagation of a hydraulic fracture, stresses are induced around the fracture tip, perturbing the in-situ stress state. There may be a fluid lag between the fluid front and the fracture tip. These phenomena help to divide the complex interaction between a hydraulic and a natural fracture into two time periods: pre-fluid front arrival and post-fluid front arrival.

Two modes of interaction occur during the pre-fluid front arrival when the fracture tip arrives at the interface. At this moment, the natural fracture is already under the influence of the stresses induced by the hydraulic fracture, which may either cause slippage or crossing. During the post-fluid front arrival, the fluid pressure is transmitted to the point of intersecting. If slippage occurred previously, the hydraulic fracture fluid may open up the natural fracture and flow into it provided the fluid pressure is greater than the normal stress acting on the natural fracture. As a consequence, the natural fracture provides the new channel for fracture propagation (Gu et al., 2011).

In the case where crossing occurs, if the fluid pressure is lower than the normal stress acting on the natural fracture, the hydraulic fracture remains planar and propagates across the interface. If the fluid pressure is greater than the normal stress acting on the natural fracture, the natural fracture opens up and fluid flows into it. This may cause the natural fracture to branch into the natural fracture creating a complex fracture network (Dahi-Taleghani and Olson, 2011).

Several studies have been carried out to understand the conditions under which the different modes of interaction occur. Blanton (1982) performed laboratory experiments using naturally fractured Devonian Shale blocks and hydrostone under varying stress conditions and angles of approach. The experiments showed that the hydraulic fractures only crossed the pre-existing fractures under high differential stress and a high angle of approach while under low differential stress and low angles of approach, the hydraulic fracture terminated against the pre-existing fracture. Warpinski and Teufel (1987) performed mineback experiments and laboratory tests to understand how geologic discontinuities affect hydraulic fracture propagation. Their results and analyses showed that for small disparity in the in-situ stresses, geological discontinuities that aligned to blunt the fracture also most likely dilated. For large differences in

the in-situ stresses, shear slippage and dilation is expected increasing leakoff. Zhou et al. (2008) performed fracturing experiments with cement blocks using three different types of paper (rice paper, printer paper and wrapping paper) with known coefficients of friction as the preexisting fractures. Results corroborated Blanton's (1982) experimental results. Gu et al. (2011) conducted laboratory tests on Colton sandstone in a small polyaxial test cell capable of imposing a true triaxial stress condition on the block. The results of the tests also showed the sensitivity of crossing to the intersection angle. As the intersection angle reduced from 90°, crossing became more difficult, while interface slippage became more likely to occur. Thiercelin and Makkhyu (2007) used the theory of dislocation to develop a semi-analytical model to predict the impact of natural fault reactivation on the stress field as a result of an approaching hydraulic fracture. The model showed that fault sliding reduced the tensile stress concentration on the other side of the fault, preventing the hydraulic fracture from crossing the fault. It was also pointed out that parameters that control fault response, such as inclination angle, remote stresses, interface properties, and fracture pressure, will also affect the crossing behavior. High inclination angle aided crossing while low inclination angle and a high pressure drop caused opening and sliding of the fault. Bahorich et al. (2012) used gypsum cement blocks to carry out experiments. Sandstone, glass and plaster were used as interfaces to represent cemented natural fractures. From the experiments three interactions were observed: the hydraulic fracture path was changed by the natural fracture, the hydraulic fracture propagated around a short natural fracture, and the hydraulic fracture diverted into the natural fracture. Differential stress, angle of intersection and the ratio of the hydraulic height to the natural fracture height were outlined as the factors that influenced the observed interactions.

Chuprakov et al. (2013) studied the effect of injection rate, fluid viscosity, fracture toughness, intersection angle, in-situ stresses, and permeability of the pre-existing fracture on the propagation of a hydraulic fracture across a weak discontinuity using a numerical simulator called MineHF2D. It was seen that hydraulic fractures mostly crossed the natural fracture at angles of intersection close to 90^{o}. Crossing behavior increases with increased differential stress even with low injection rate and/or viscosity, increased fluid viscosity and or injection rate and coefficient of friction. Chuprakov and Prioul (2015) developed an analytical model to investigate the hydraulic fracture height containment observed in mine and field experiments when hydraulic fractures intersect weak formation bedding planes. The model estimates fracture blunting, slippage of the interface and predicts the net pressure build up required for crossing. Results from the model showed that at the point of contact, the fracture becomes compliant elastically which causes an increase in volume, a corresponding decrease in net pressure and elastic energy and thus fracture propagation is halted. Crossing will be dependent on the future net pressure buildup and degree of interface weakening caused by the infiltration of the hydraulic fracture fluid.

1.3 BACKGROUND ON CROSSING CRITERIA

Renshaw and Pollard (1995) developed a model to predict the propagation of a hydraulic fracture across an orthogonal frictional interface by using linear elastic fracture mechanics (LEFM) to determine the stresses near the fracture tip. Crossing was assumed to occur by re-initiation of new fractures on the opposite end of the interface and not by the continuous propagation of the hydraulic fracture across the interface. This assumption is supported by the spatial offset observed across an interface when a hydraulic fracture crosses it (Helgeson and

Aydin 1991; Heuze et al., 1990). Chuprakov et al (2011) numerically simulated the stress induced along the natural fracture before and after the fluid front arrival in the hydraulic fracture. By monitoring the tensile peaks along the natural fracture, it was found that a new tensile fracture perpendicular to the natural fracture may be formed on the other side of the natural fracture due to the induced tensile stress. The increase of the tensile peaks with increased differential far-field stress and natural fracture angle is consistent with experimental results for crossing by Blanton (1982). Renshaw and Pollard's (1995) model also assumed that the interface does not change the direction of propagation and that the fluid pressure is not large enough to cause the hydraulic fracture to turn into the interface (He et al., 1989). The crossing criterion proposed that crossing across an interface will only occur if the compression acting perpendicular to the interface if sufficiently large enough to prevent the interface from slipping and if the induced stresses ahead of the fracture tip is sufficient enough to initiate a new tensile fracture on the opposite end of the interface. The crossing condition for a hydraulic fracture propagation in the x-axis is:

$$\frac{-\sigma'_{xx}}{T_o - \sigma'_{yy}} > 0.33\left[1 + \frac{1}{\mu}\right] \tag{1.1}$$

where σ'_{xx} is the Terzaghi effective maximum principal stress, σ'_{yy} is the Terzaghi effective minimum principal stress, T_o is the tensile strength of the matrix on both ends of the interface and μ is the coefficient of friction along the interface.

Gu and Weng (2010) extended Renshaw and Pollard's criterion for orthogonal intersections to non-orthogonal intersections and developed a simple algorithm involving quadratic equations to determine if slip occurs for given stress states, mechanical properties and natural fracture orientation. The no-slip interface condition was:

$$|\tau_\beta| < S_o - \mu\sigma_{\beta y} \quad (1.2)$$

where τ_β and $\sigma_{\beta y}$ are the shear and normal stresses on the interface respectively, S_o is the cohesion of the interface while μ is the coefficient of friction.

1.4 OBJECTIVE

The objective of this thesis is to develop a novel technique for lost circulation mitigation in low permeability formations based around the idea of encouraging termination of hydraulic fractures against natural fractures and bedding planes. The following was done:

- Developed and tested the novel hypothesis of how low matrix permeability could encourage termination through a time-dependent poroelastic effect
- Developed a time and permeability based crossing criterion
- Utilized the crossing criteria for the design of novel lost circulation mitigation procedures

1.5 PROPOSED CONCEPT

Figure 1.1 shows a map view of the proposed lost circulation mitigation concept. The black line signifies the wellbore, red lines signify the hydraulic fractures, and the blue line signifies the natural fractures. As the hydraulic initiates from the wellbore during drilling, it propagates until it terminates against a natural fracture. With continued flow, new hydraulic fractures are initiated from the natural fracture and propagate until they come in contact with another natural fracture where termination occurs again and another new set of hydraulic

fractures are initiated. This process is repeated until a dendritic fracture network is formed around the wellbore.

After the formation of the fracture network, it is then plugged up with highly viscous fluids which prevent the further propagation of the fracture network during drilling.

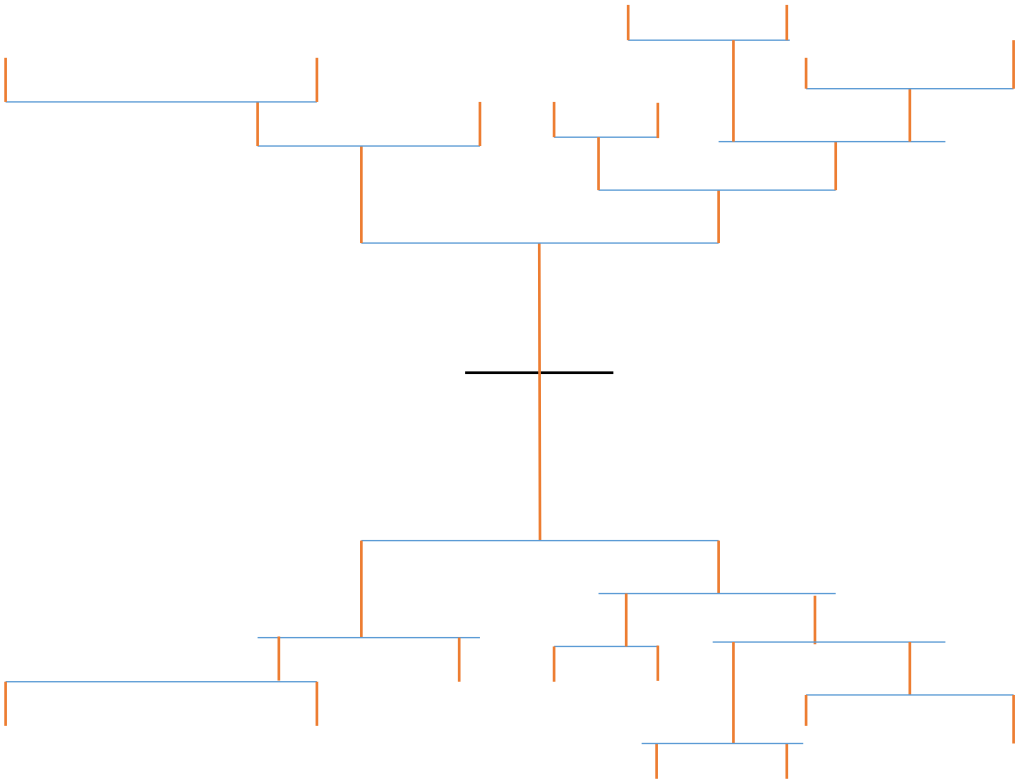

Figure 1.1: Map view showing the fracture network to be generated for the proposed lost circulation mitigation concept

1.6 OUTLINE OF THE THESIS

Chapter 2 describes the complex fracture simulator (CFRAC) used in this work. Chapter 3 explains the physics behind poroelastic effect hypothesis and shows the verification of the

hypothesis by subjecting a fracture to an instantaneous change in normal stress. In Chapter 4, the fracture is subjected to a gradual change in normal stress. Chapter 4 shows a sensitivity study carried out to study the effect of propagation rate, tensile yield stress, and permeability on the tendency for new fractures to initiate on the other side of the frictional interface. Chapter 5 provides a numerical investigation of the proposed lost circulation mitigation technique.

Chapter 2 : How CFRAC works

The simulations performed for this study used a simulator called CFRAC, Complex Fracture ReseArch Code (McClure, 2012). CFRAC fully couples fluid flow and stresses induced by fracture deformation in large, discrete fracture network models. A brief summary of the equations solved by CFRAC is given in this chapter. A more detailed description is given by McClure (2012).

CFRAC simulates fluid flow in discrete fracture networks (DFN), with leakoff from the fracture into the surrounding matrix and vice-versa. Fluid flow is isothermal and single-phase liquid with no gravity effects. The fluid has a constant viscosity and is slightly compressible. The boundary condition for fluid flow at the wellbore is either constant rate or constant pressure with no flow across the edges of the spatial domain. CFRAC uses the cubic law (Witherspoon et al., 1980) to solve the unsteady mass balance equation in the fractures:

$$\frac{\partial(\rho E)}{\partial t} = \nabla \cdot \left(\frac{\rho}{\mu}\frac{e^3}{12}\frac{dP}{dx}\right) + F_{fm} + s_f \tag{2.1}$$

where s_f is a source term depicting a well, t is time, E is the void aperture, e is the hydraulic aperture, ρ is fluid density, x is distance along the fracture, F_{fm} is the mass rate of leakoff, P is pressure, μ is fluid viscosity, and k is permeability. The simulator uses Darcy's law to solve the unsteady mass balance equation in the matrix:

$$\frac{\partial(\rho\phi)}{\partial t} = \nabla \cdot \left(k\frac{\rho}{\mu}\nabla P\right) - F_{fm} + s_m \tag{2.2}$$

where ϕ is the porosity and s_m is a source term depicting a well. Fluid flow in the matrix and the fractures and the mass transfer between the fractures and the matrix is calculated using the finite

volume method. From the cubic law (Witherspoon et al., 1980), fracture transmissivity is evaluated as:

$$T = \frac{e^3}{12} \tag{2.3}$$

where e is the hydraulic aperture.

An unstructured meshing program called Traingle (Shewchuk, 1996) is used for the matrix meshing. For accuracy of the mechanical calculations it is necessary for the fracture element lengths to be constant or varying smoothly, hence a different algorithm is used to ensure constant node spacing along the fracture. The causes the mesh to be fully conforming with the edges of the matrix elements perfectly coinciding with neighboring matrix and fracture elements.

Another option for describing leakoff is Vinsome and Westerveld's (1980) semianalytical method. It was originally created to model the heat loss due to conduction into a cap rock. The single phase fluid flow in a porous media assuming constant viscosity, compressibility and permeability is similar to the equation for heat conduction. Hence, Vinsome and Westerveld's (1980) can be applied to porous media by replacing the heat conduction variables with the corresponding porous media variables. This model assumes a 1D leakoff and that the leakoff from each element is independent of the leakoff from other surrounding elements. It ignores the poroelastic fluid pressure response in the formation due to deformation at the fractures. The Vinsome and Westerveld's (1980) model is preferable to the Carter leakoff model (Howard and Fast, 1957) because it captures accurately the variation of fracture pressure with time.

In CFRAC, fractures are defined as "closed" if the fractures walls are touching and the normal stress is greater than the fluid pressure. Fractures are defined as "open" if the walls are not touching because the fluid pressure has become equal to the normal stress. For smooth surfaces, the hydraulic aperture, e, and void aperture, E, are equal. However, for rough fractures,

these values may differ. CFRAC allows E and e to be different and uses the Willis-Richards et al. (1996) model based on the work of Barton et al. (1985) to calculate the aperture of closed fractures:

$$E = \frac{E_0}{1+\frac{9\sigma'_n}{\sigma_{n,Eref}}} \tag{2.4}$$

where σ_n is the normal stress, E_0 is the void aperture at zero effective stress, $\sigma_{n,Eref}$ is the 90% closure stress and σ'_n is the effective normal stress. Similarly, hydraulic aperture is calculated as:

$$\mathrm{e} = \frac{e_0}{\left(1+9\sigma'_\mathrm{n}/\sigma_{eref}\right)} + \mathrm{D_s} \times \tan\left(\frac{\phi_{\mathrm{edil}}}{1+\frac{9\sigma'_\mathrm{n}}{\sigma_{eref}}}\right) \tag{2.5}$$

where e_0 is the hydraulic aperture at zero effective normal stress and shear sliding displacement, σ_{eref} is the effective normal stress that causes a 90% reduction in the hydraulic aperture, ϕ_{edil} is the shear dilation angle, and D_s is the cumulative sliding displacement. For open fractures:

$$E = E_0 + E_{open} \tag{2.6}$$

where E_{open} is the mechanical opening (the degree of separation between the fracture walls when opening occurred). Mechanical boundary conditions are imposed in the fractures. For open fractures:

$$\sigma_n - P = 0 \tag{2.7}$$

$$\tau = 0 \tag{2.8}$$

where τ is the shear stress. For closed fractures, Coulomb failure law is used to predict sliding:

$$|\tau - \eta v| \leq (\sigma_n - P)\mu + S_0 \tag{2.9}$$

where P is the pressure inside the fracture, μ is the coefficient of friction, S_0 is the fracture cohesion, and ηv is a radiation damping term for the effect of high slippage velocity inertial (Segall, 2010).

Stresses induced by fracture deformation are calculated using the boundary element displacement discontinuity method described by Shou and Crouch (1995). The calculations assume that the medium is homogeneous, infinite, isotropic and linearly elastic. The propagation of hydraulic fractures is treated using linear elastic fracture mechanics. The mode I stress intensity factor, K_I, is calculated numerically. The fracture will only propagate if the stress intensity facture reaches the fracture toughness, K_{Ic}.

Ma (2015) added the ability to simulate polymer transport and complex fluid rheology to CFRAC. The finite volume method is used to solve the unsteady polymer mass balance equation in a fracture:

$$\frac{\partial(EC_p)}{\partial t} + \nabla \cdot \left(u_{flux} e C_p\right) = 0 \tag{2.10}$$

where $C_p$is the polymer concentration for a single fracture element, u_{flux} is the volumetric fluid flux and e is the hydraulic aperture; and also the unsteady polymer mass balance in the matrix:

$$\frac{\partial(\phi C_p)}{\partial t} + \nabla \cdot \left(u_{flux} C_p\right) = 0 \tag{2.11}$$

where ϕ is the porosity. The model ignores polymer dispersion, adsorption and degradation, fluid density is assumed to be independent of polymer concentration while salinity is kept at a

constant value. Implicit iterative coupling is used for the coupling of polymer concentration with viscosity. Viscosity can be calculated using two different methods:

- A simple linear relationship between viscosity and polymer concentration

$$\mu_{app} = A_{mat} C_p + \mu_w \tag{2.12}$$

$$\mu_{app} = A_{frac} C_p + \mu_w \tag{2.13}$$

where μ_{app} is apparent viscosity, C_p is polymer concentration, μ_w is water viscosity (set to 1 cp), A_{mat} and A_{frac} are two linear coefficients for matrix and fracture flow, respectively.

- Rheology model for HPAM using the unified model developed by Delshad et al. (2008), which combines both shear thining and thickening rheology functions for flow in a porous media and Carreau (1972) equation for flow in the fractures:

$$\mu_{app} = \mu_w + \left(\mu_p^0 - \mu_w\right)\left[1 + (\lambda \dot{\gamma}_{eff})^2\right]^{(n-1)/2} \tag{2.14}$$

where μ_p^0 is the zero shear rate viscosity, $\dot{\gamma}_{eff}$ is the apparent shear rate and *n* is an exponent equal to 0.78.

Chapter 3 : Fracture Subjected to Instantaneous Stress Change

3.1 INTRODUCTION

As an initial step, we performed simulations of the fluid pressure and aperture evolution in a single isolated crack subjected to an instantaneous stress change. In reality, the stress on the fracture would change over time as the hydraulic fracture approached, but we chose to start with this simplified calculation.

3.2 METHODOLOGY

Figure 3.1 shows the normal stress history imposed on the fracture in the simulations. Figure 3.2 shows the expected poroelastic pressure response in the incipient fracture in response to the imposed stress change.

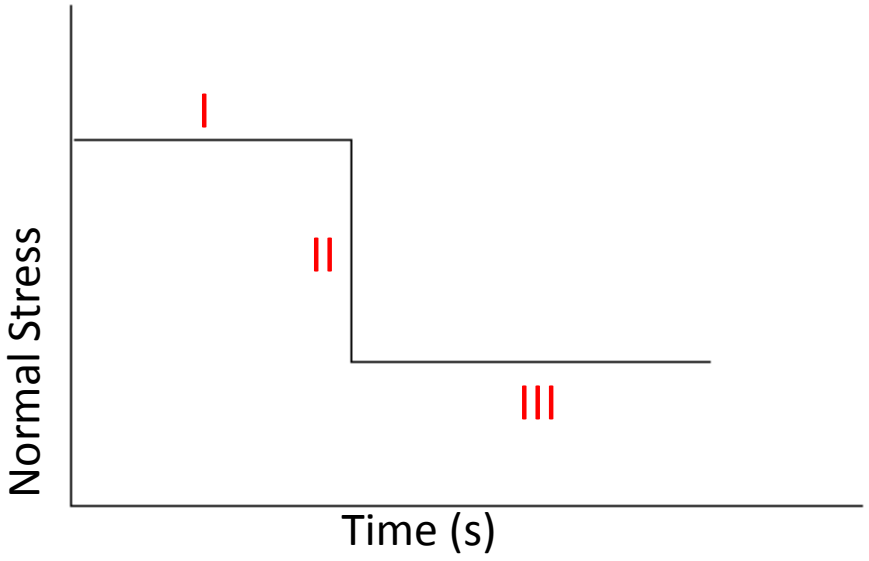

Figure 3.1: Simulated variation in normal stress

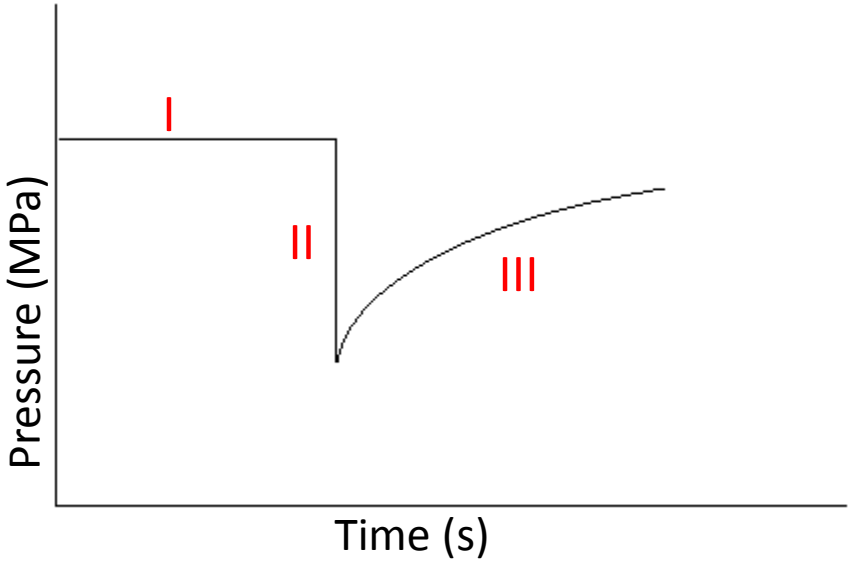

Figure 3.2: Poroelastic pressure profile in a fracture in response to the variation in normal stress shown in Figure 3.1

In region I, the normal stress is greater than the pressure inside the incipient fracture so the fracture remains closed and pressure remains constant. In region II, an instantaneous decrease in the normal stress (below the pressure in fracture) is imposed on the fracture and the fracture tries to open. Since the fluid in the fracture is assumed to be water which is only slightly compressible (only a small change in density with changes in pressure), the opening of the fracture creates a sharp pressure drop. This occurs because the fracture cannot open further because of mass conservation. With the normal stress maintained at the reduced value in region III, fluid begins to flow into the fracture from the matrix, and pressure in the fracture begins to build up. This is evident in the increasing pressure trend in region III.

The simulations were performed to predict the pressure in region III. This was done by initializing the normal stress (19 MPa) to be lower than the matrix pressure (30 MPa) and using the full triangular mesh option of CFRAC as shown in Figure 3.3 to simulate flow into the

fracture in order to produce the poroelastic pressure response. Since the flow into the fracture is a function of permeability, a sensitivity analysis was done to investigate the effect of permeability on the stress intensity factor that develops on the incipient fracture. Three different lengths for the incipient fracture were investigated. The effect of the matrix pressure on the stress intensity factor was also investigated.

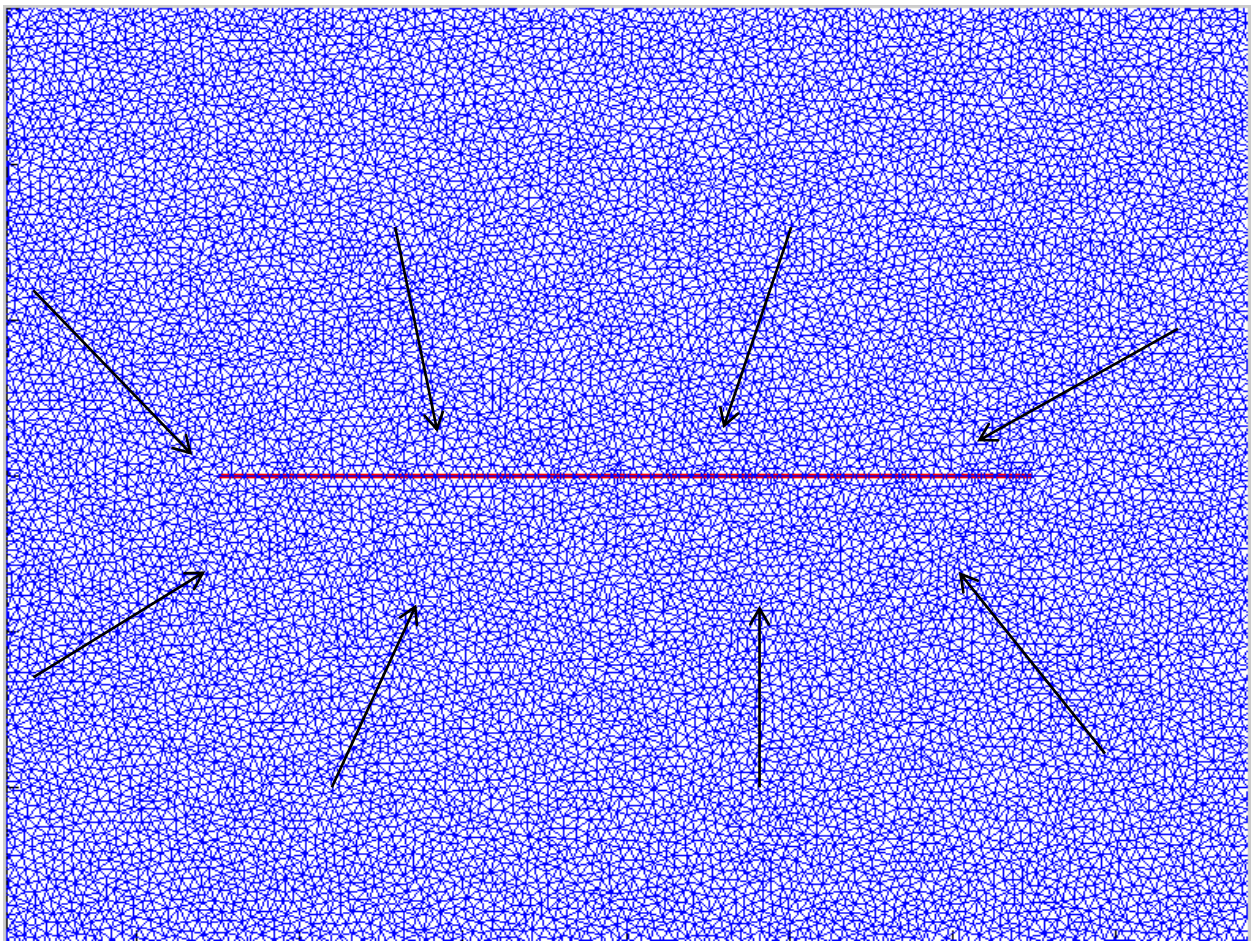

Figure 3.3: Map view showing the full triangular mesh (blue lines) around a fracture (red line) and the direction of fluid flow (black arrows)

Table 3.1: Simulation parameters that were held constant in all simulations

Parameter	**Value**	**Units**
σ_{yy}	19	MPa
σ_{xx}	19	MPa
σ_{xy}	0	MPa
G	15000	MPa
P_{init}	30	MPa
$pinjmax$	60	MPa
υ	0.25	unitless
h	100	m
μ	0.6	unitless
S_o	0.5	MPa
K_{Ic}	2	$MPa.m^{1/2}$
ϕ_{Edil}	0.0	degrees
e_0	0.0000001	unitless
E_0	0.000000001	unitless
μ_f	1	cp
ϕ_i	0.03	unitless
c_ϕ	0.00145	MPa^{-1}
c_w	0.000458	MPa^{-1}
ϕ_{edil}	0.0	degrees
η	3	MPa/(m/s)

Table 3.1: (Continued)

$\sigma_{n,eref}$	20	MPa
$\sigma_{n,Eref}$	20	MPa

Table 3.2: Simulation parameters that were varied in the simulations

Parameter	**Value(s)**
k	1 mD, 10 μD, 100 nD
Incipient fracture length	1 mm, 5 cm, 1 m
P_{init}	30 MPa, 25 MPa, 20 MPa

3.3 RESULTS AND DISCUSSION

3.3.1 Case I: Smallest incipient fracture length (1 mm)

Figure 3.4, Figure 3.5, and Figure 3.8 show simulations results for a 1 mm fracture and three different values of matrix permeability. The plots show that the time required for the fracture aperture and K_I to rise was greater for lower permeability. The small size of the fracture in these simulations (1 mm) limited the fracture aperture and the magnitude of K_I, which peaked at less than 0.5 MPa.m$^{1/2}$.

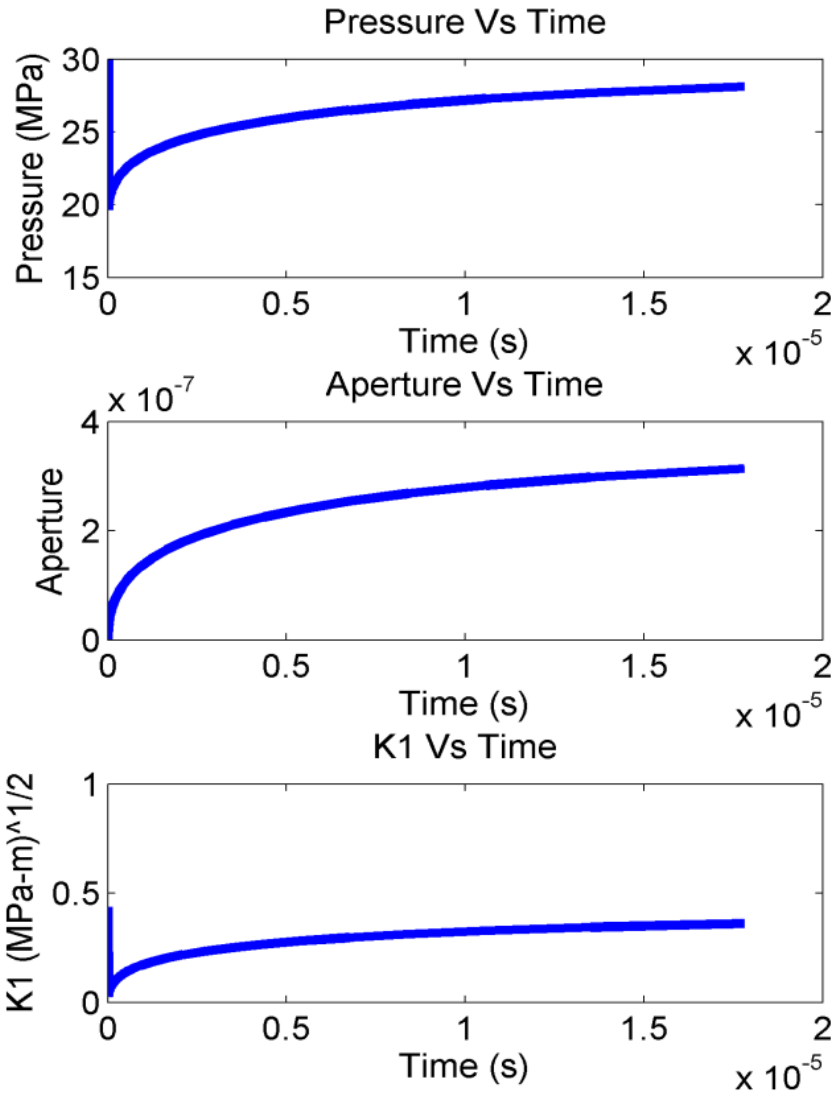

Figure 3.6: Plot of pressure, aperture and K_I versus time for a fracture of length 1 mm, matrix pressure of 30 MPa, and matrix permeability of 1 mD

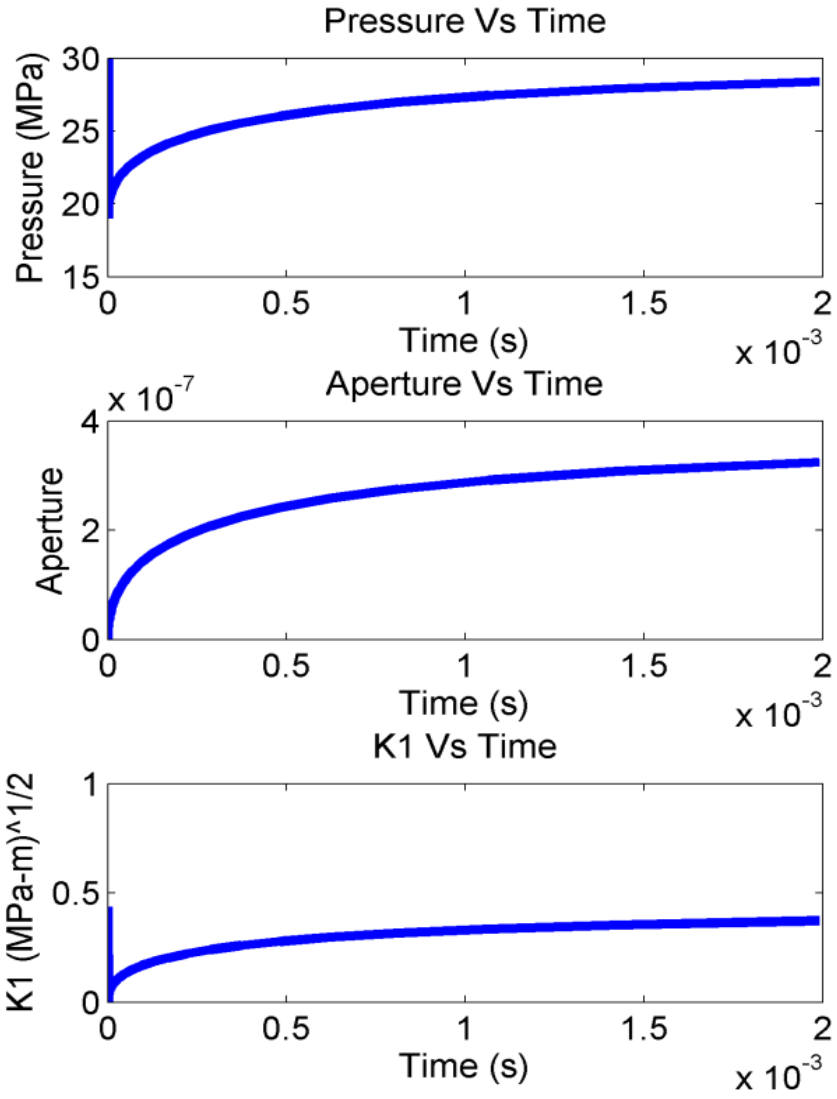

Figure 3.7: Plot of pressure, aperture and K_I versus time for a fracture of length 1 mm, matrix pressure of 30 MPa, and matrix permeability of 10 μD

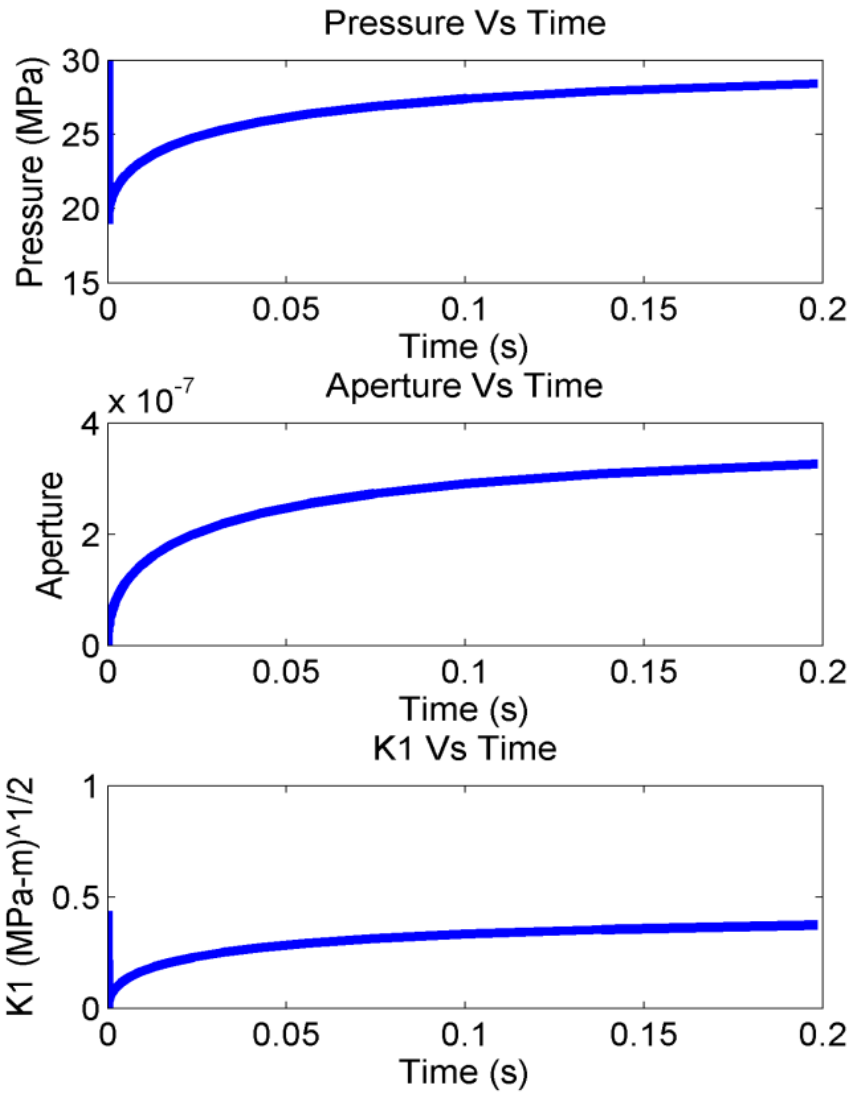

Figure 3.8: Plot of pressure, aperture and K_I versus time for a fracture of length 1 mm, matrix pressure of 30 MPa, and matrix permeability of 100 nD

3.3.2 Case II: Intermediate incipient fracture length (5 cm)

In case II, fracture length was assumed to be 5 cm. As in case I, three simulations were run with three different values of permeability. Similar pressure, aperture and K_I profiles were observed. The main difference was that it took a longer time for pressure to build up in the fracture and reach the peak value of K_I. For the low permeability (100 nD), even though K_I reached K_{Ic}, it took several minutes for this to occur.

The buildup of pressure was slower because fracture compliance is proportional to size (either length, height, or radius, depending on geometry). Thus, the volume of fluid required to fill a fracture to a given pressure scales with the square of the fracture size. The volume per fracture area required to fill a fracture scales linearly with fracture size.

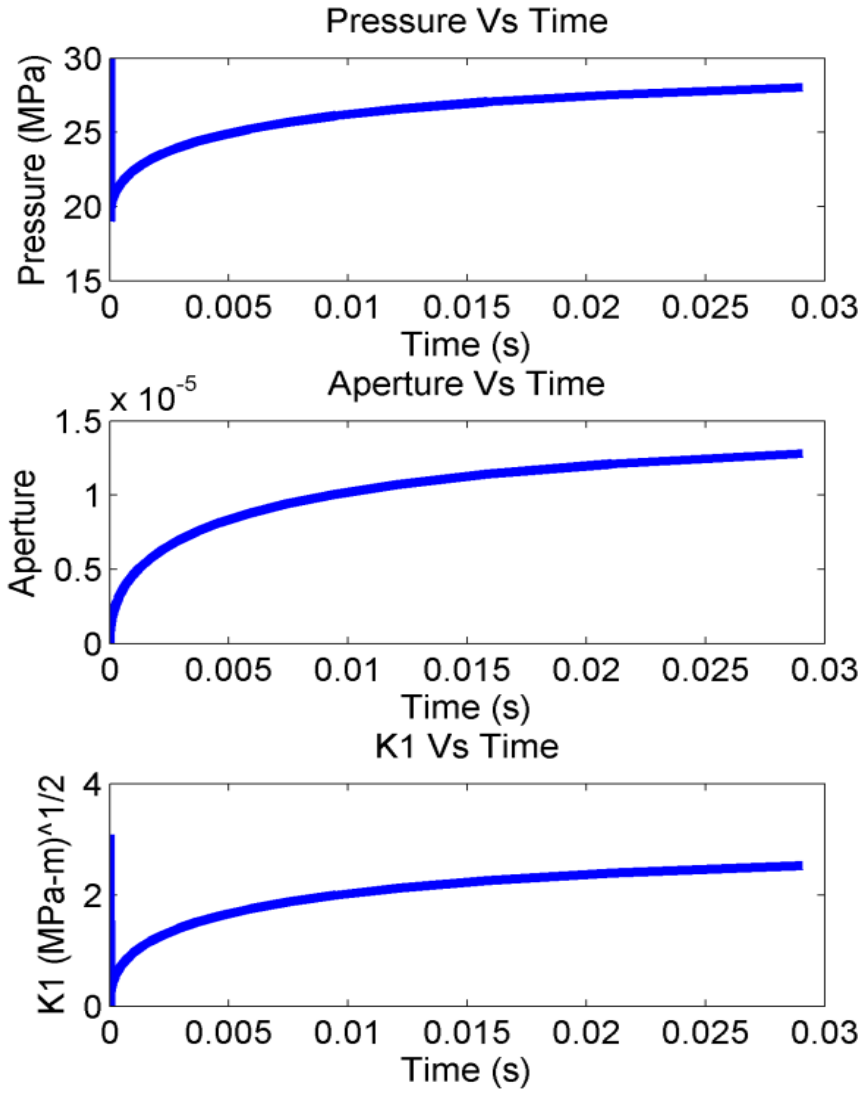

Figure 3.9: Plot of pressure, aperture and K_I versus time for a fracture of length 5 cm, matrix pressure of 30 MPa, and matrix permeability of 1 mD

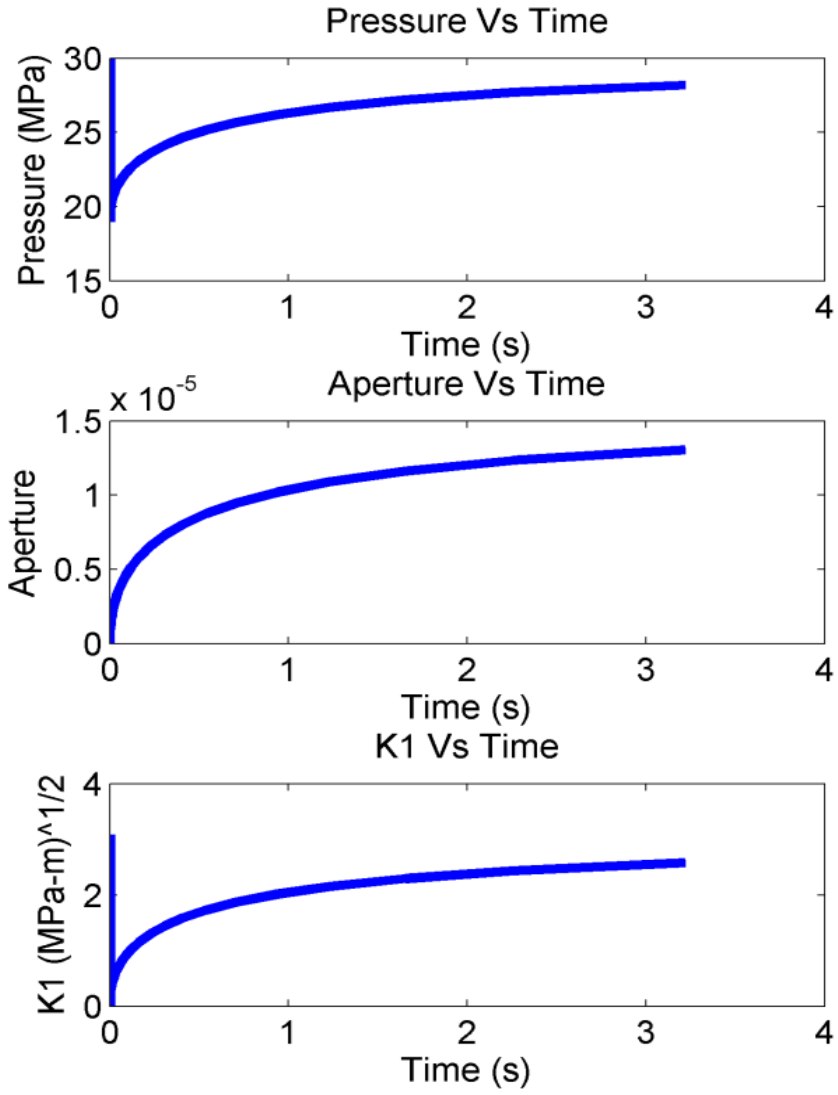

Figure 3.10: Plot of pressure, aperture and K_I versus time for a fracture of length 5 cm, matrix pressure of 30 MPa, and matrix permeability of 10 μD

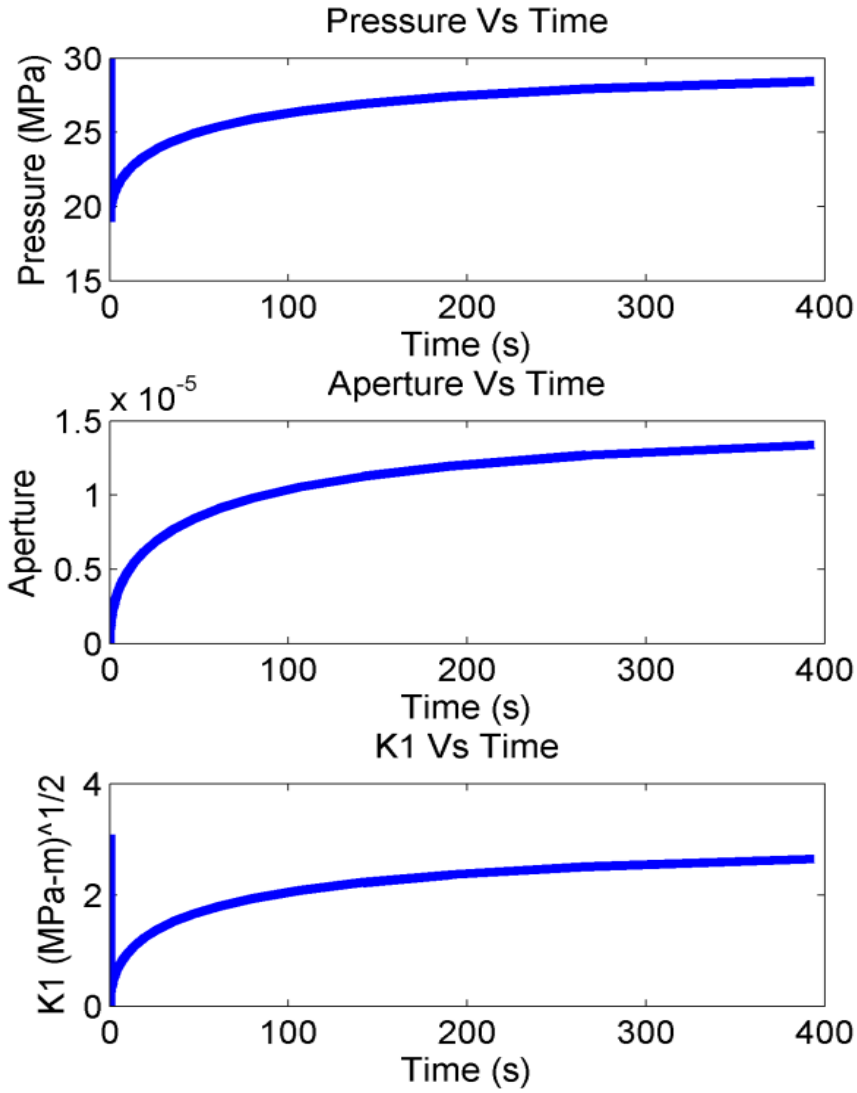

Figure 3.11: Plot of pressure, aperture and K_I versus time for a fracture of length 5 cm, matrix pressure of 30 MPa, and matrix permeability of 100 nD

3.3.3 Case III: Largest incipient fracture length (1 m)

The amount of time required for pressure to build up in the fracture further increased in case III, which used the largest incipient fracture length (1 m). In reality, the value of K_I would

not be able to exceed K_{Ic} as it did in these simulations (reaching a value of about 10 MPa.m$^{1/2}$) because the fracture would propagate once K_I reached K_{Ic}.

In cases I, II, and II, the fracture length of 5 cm (case II) was the most favorable for fracture crossing. If the incipient fracture was too small, K_I could not reach the fracture toughness. But if the fracture was too long, it took a very long time to reach K_{Ic}.

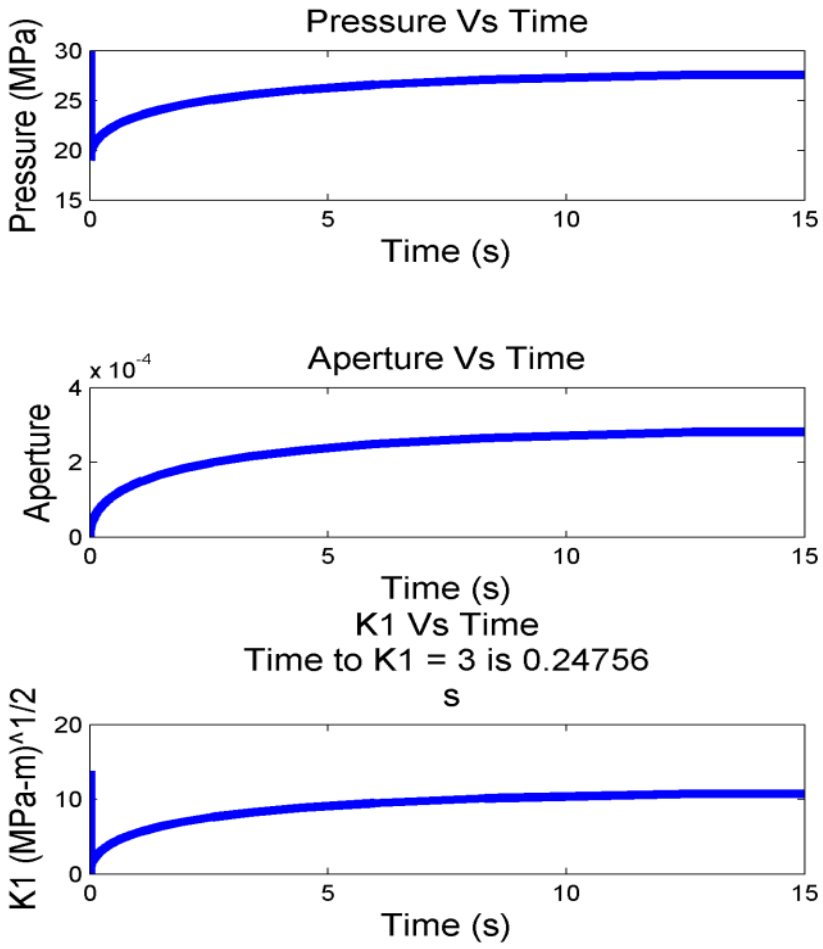

Figure 3.12: Plot of pressure, aperture and K_I versus time respectively of the opening of a fracture of length 1m, matrix pressure of 30 MPa, and matrix permeability of 1 mD

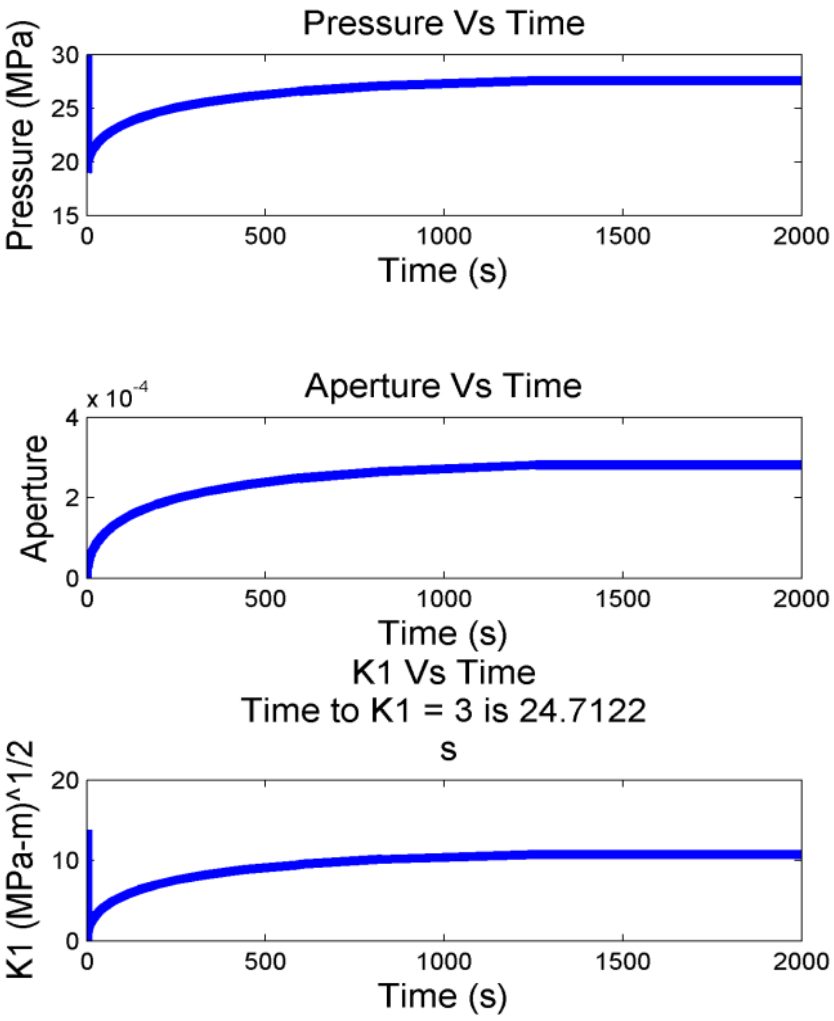

Figure 3.13: Plot of pressure, aperture and K_I versus time respectively of the opening of a fracture of length 1m, matrix pressure of 30 MPa, and matrix permeability of 10 μD

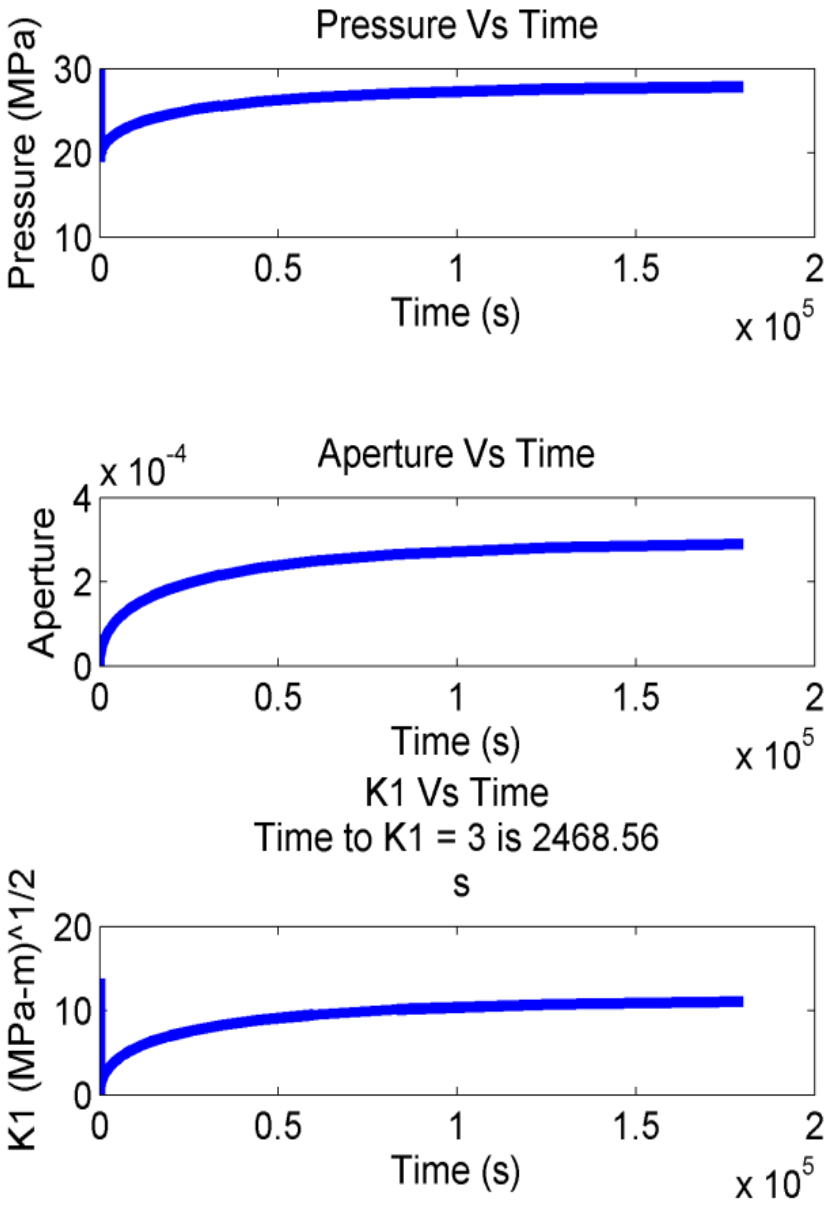

Figure 3.14: Plot of pressure, aperture and K_I versus time for a fracture of length 1m, matrix pressure of 30 MPa, and matrix permeability of 100 nD

3.3.4 Case IV: Intermediate incipient fracture length (5cm)

Three additional simulations were performed to investigate the effect of remote loading net pressure (initial normal stress minus fluid pressure). For lower values of initial fluid pressure and initial net pressure, the degree of fracture opening (aperture) and K_I reduced.

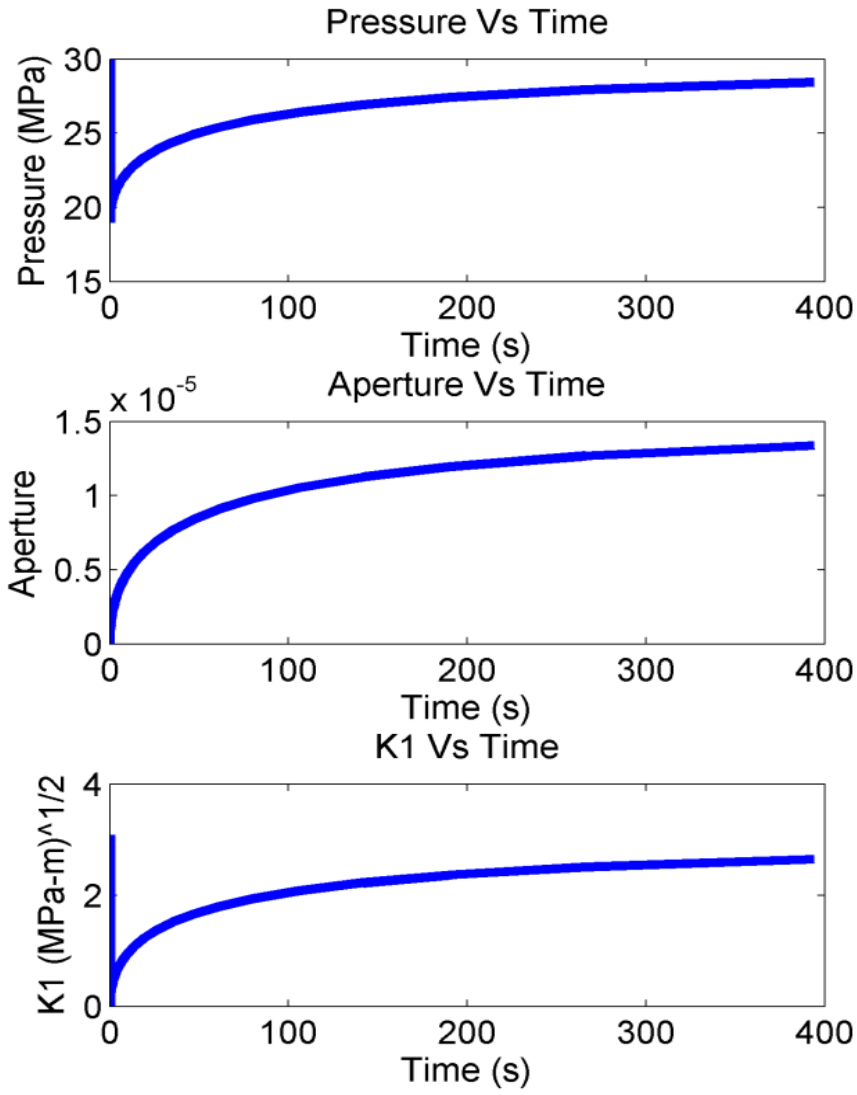

Figure 3.15: Plot of pressure, aperture, and K_I versus time respectively for an incipient fracture length of 5 cm, matrix pressure of 30 MPa, and matrix permeability of 100 nD

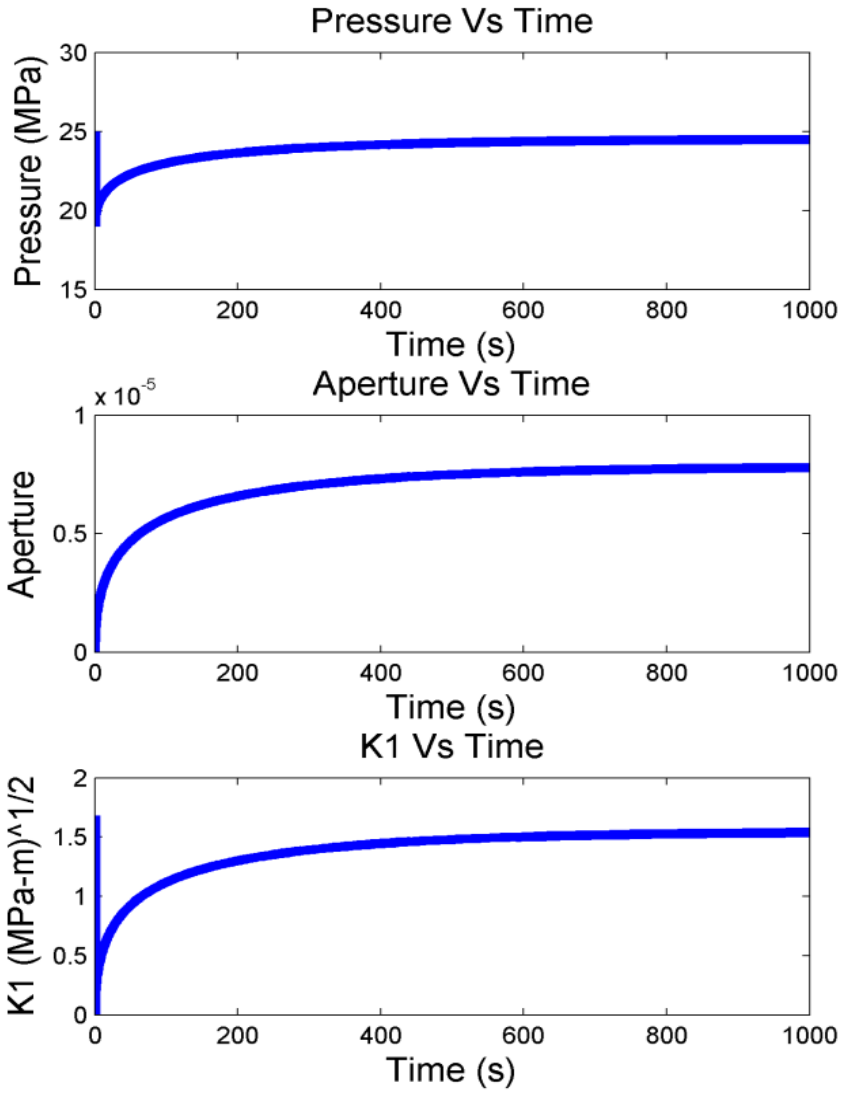

Figure 3.16: Plot of pressure, aperture, and K_I versus time respectively for an incipient fracture length of 5 cm, matrix pressure of 25 MPa, and matrix permeability of 100 nD

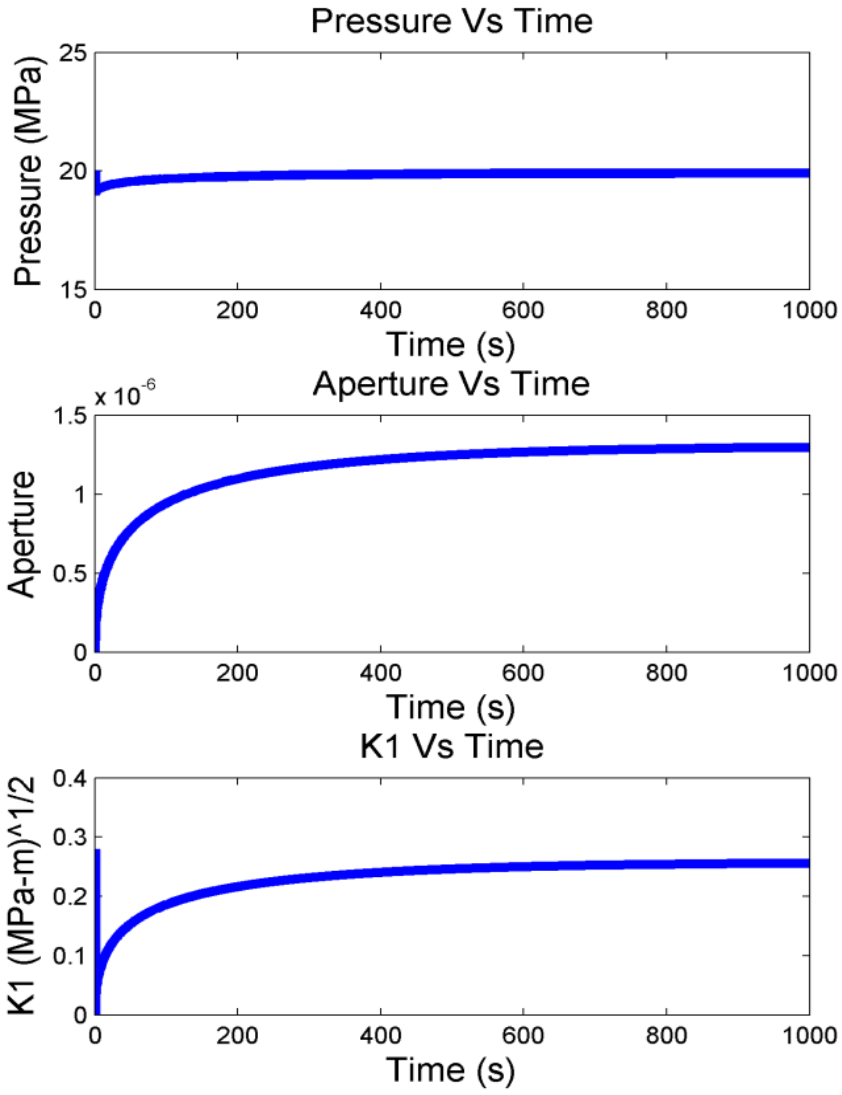

Figure 3.17: Plot of pressure, aperture, and K_I versus time respectively for an incipient fracture length of 5 cm, matrix pressure of 20 MPa, and matrix permeability of 100 nD

As matrix pressure reduced from 30 MPa to 20 MPa, the degree of fracture opening (aperture) reduced alongside the values of K_I. Because of the low values of K_I for the 25MPa and 20 MPa cases, the fracture would not propagate, which implies that crossing would not occur.

3.4 CONCLUSION

At low enough permeability, it may take minutes or more for incipient fractures to initiate on the other side of the natural fracture. During that time, the propagating hydraulic fracture may reach the fracture and blunt, and fluid may divert into the natural fracture. This suggests that crossing may be less likely to occur in low permeability formations and the rapidly propagating hydraulic fractures may be more likely to terminate.

Chapter 4 : Sensitivity Study

4.1 INTRODUCTION

In the previous chapter, an instantaneous drop in the normal stress was imposed on the incipient fracture. In this chapter the incipient fracture is subjected to time-varying stress, simulating the approach of a hydraulic fracture. The sensitivity analysis investigated the effect rate of propagation, tensile strength, and permeability on the stress intensity factor that develops on the incipient fracture.

4.2 METHODOLOGY

In order for the sensitivity analysis to be carried out, the variation of the normal stress on the incipient fracture was estimated by considering the effect of the approaching hydraulic fracture. The size of the process zone ahead of the hydraulic fracture and the length of the incipient fracture were also estimated.

4.2.1 Effect of the approaching hydraulic fracture on the incipient fracture

As a hydraulic fracture propagates, deformation induced by the fracture perturbs the in-situ stress state around the fracture. In a formation, the in-situ stresses acting are compressional. As a hydraulic fracture approaches an incipient fracture, the stresses acting on the incipient fracture gradually become less compressive (more tensile), and eventually the fluid pressure may exceed the minimum principal stress.

The full stress field equation for a mode I fracture (Pollard and Segall 1987) given below was used to estimate the induced stress σ_{yy} at a distance, r, from the hydraulic fracture.

$$\sigma_{yy} = \sigma_{yy}{}^{r} - \left(P_{frac} - \sigma_{yy}{}^{r}\right)\left[rR^{-1}\cos(\theta - \Gamma) - 1 + L_f rR^{-3} sin\theta sin3\Gamma\right] \quad (4.1)$$

where,

$$R = \sqrt{r_1 r_2} \quad (4.2)$$

$$\Gamma = \frac{\theta_1 + \theta_2}{2} \quad (4.3)$$

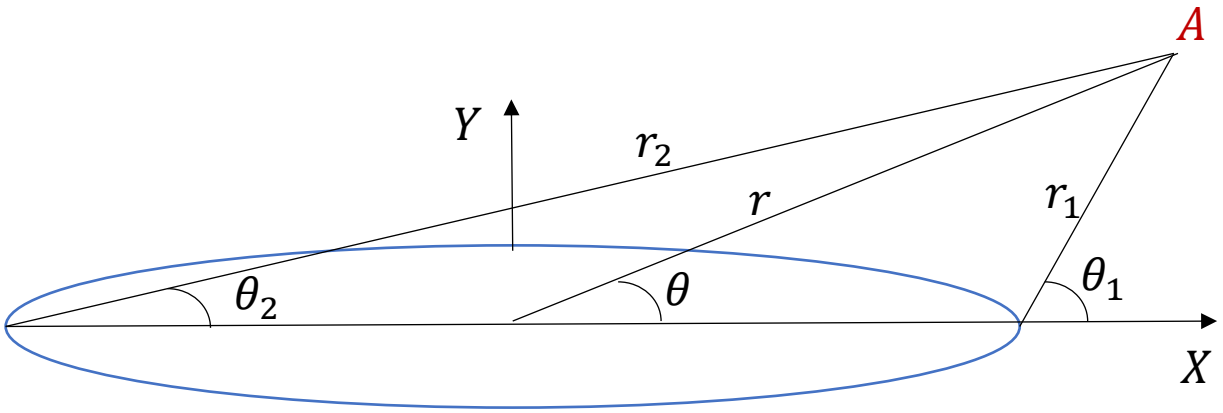

Figure 4.1: Schematic used to estimate σ_{yy} at a point A away from a hydraulic fracture (blue line)

For a fracture propagating parallel to its axis, θ = 0, hence θ_1 and θ_2 = 0. Therefore the equation reduces to:

$$\sigma_{yy} = \sigma_{yy}{}^{r} - \left(P_{frac} - \sigma_{yy}{}^{r}\right)\left[\frac{r + L_f}{\sqrt{2L_f r + r^2}} - 1\right] \quad (4.4)$$

The equation above was modified to obtain a time dependent variation of σ_{yy} and is illustrated below.

Consider a hydraulic fracture of initial half length, L_{f_i} initially at a distance r_i from the natural fracture is propagating with a velocity, v, towards an incipient fracture of half length L_{f_c} as shown in the figure below.

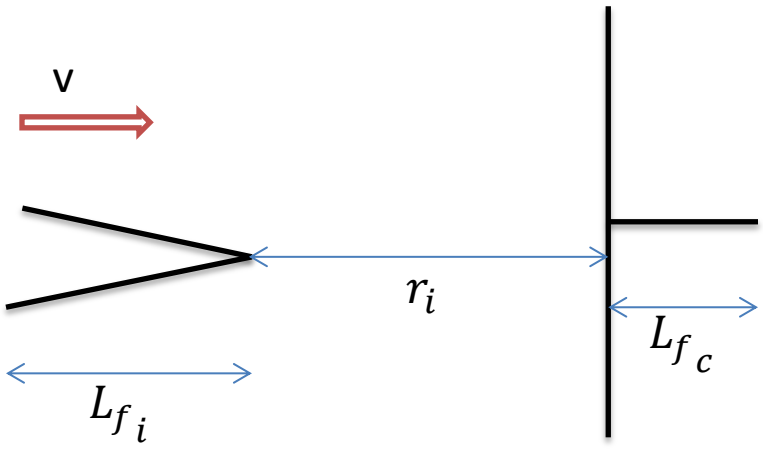

Figure 4.2: Schematic for the derivation of time varying σ_{yy}

$$r = r_i - vt \tag{4.5}$$

$$L_f = L_{f_i} + vt \tag{4.6}$$

Replacing r and L_f in eqn (4.4) with the expressions above respectively, eqn (4.4) becomes:

$$\sigma_{yy} = \sigma_{yy}{}^{r} - (P_{frac} - \sigma_{yy}{}^{r})\left[\frac{r_i + L_{f_i}}{\sqrt{r_i\left(2L_{f_i} + r_i\right) - (2L_{f_i}vt + (vt)^2)}} - 1\right] \tag{4.7}$$

This expression estimates σ_{yy} on the incipient fracture taking into account the induced tensile stress of the approaching hydraulic fracture.

4.2.2 Size of the process zone

The region around the fracture tip can be divided in two regions: the region of induced tension (further from the fracture tip) and the region of highest tensile stress, known as the process zone. From eqn (4.7), σ_{yy} is proportional to $1/\sqrt{r_i}$ which means that there is a singularity at the fracture tip. This does not occur in reality. Microcracks are formed around the fracture tip (Friedman et al. 1971) as a result of the high tensile stress in this region and thus prevent the stress singularity from occurring. In this work, the process zone was assumed to be the region of tensile failure where $\sigma_{yy} - P$ was equal to $-T_0$, the tensile strength of the formation. Thus, Equation 4.7 is used for calculating the stress induced ahead of the approaching fracture. But once $\sigma_{yy} - P_{init}$ reaches $-T_0$, the value of σ_{yy} is not permitted to decrease further and is held constant. If the process zone was not included in the calculation, then the value of σ_{yy} would approach $-\infty$ as the crack tip approached.

4.2.3 Optimum Length for the incipient fracture

If the length of an incipient fracture is too small, the stress intensity factor will reach not the fracture toughness required for propagation. Conversely, if the length is too long, it will take a long period of time for an incipient fracture to be re-pressurized. The optimum length was estimated using the equation for calculating the stress intensity factor of a plane strain fracture with constant internal pressure and remote compressive stress:

$$K_I = (P_{frac} - \sigma_{yy})\sqrt{\pi\, L_{f_c}} \tag{4.8}$$

where P_{frac} is the fluid pressure inside the incipient fracture and L_{f_c} is the length of the incipient fracture.

The minimum possible length of a fracture where K_I can reach K_{Ic} is found by solving Equation 4.8 for L_{f_c} assuming K_I is equal to K_{Ic} and that P_{frac} is the equal to the in-situ matrix fluid pressure. For fracture propagation, the effective stress must be equal to the tensile strength of the formation, implying:

$$\sigma_{yy} - \ Matrix\ pressure = Tensile\ Strength\ (T) \tag{4.9}$$

Making the necessary substitution, the equation of the optimum length is given by:

$$L_{f_c} = \frac{1.5\ {K_{Ic}}^2}{\pi T^2} \tag{4.10}$$

As shown in Chapter 3, the fracture pressure asymptotically approaches P_{init} in response to a stress perturbation. Therefore, if the fracture is only the minimum possible length, it could take a long time for the pressure to rise high enough to cause propagation. So L_{f_c} is multiplied by 1.5 so that the fracture does not need to reach pressure equal to P_{init} in order to propagate.

4.2.4 Simulation setup

The simulation setup is similar to Chapter 3. The major difference is that the incipient fracture is subjected to decreasing normal stress as a result of the approaching hydraulic fracture. The normal stress decreases until it becomes tensile and reaches an imposed limit. Since the

stress in the process zone is assumed to be constant and equal to the tensile strength of the rock, the tensile strength serves as the imposed limit for the normal stress.

Table 4.1: Simulation parameters that were held constant in all simulations

Parameter	**Value**	**Units**
σ_{yy}	27	MPa
σ_{xx}	27	MPa
σ_{xy}	0	MPa
P_{init}	17	MPa
P_{frac}	30	MPa
$pinjmax$	60	MPa
L_{f_i}	5	m
r_i	13	m
G	15000	MPa
υ	0.25	unitless
h	100	m
μ	0.6	unitless
S_o	0.5	MPa
ϕ_{Edil}	0.0	Degrees
e_0	0.0000001	unitless
E_0	0.0000001	unitless

Table 4.1: (Continued)

μ_f	1	cp
ϕ_i	0.03	unitless
c_ϕ	0.00145	MPa^{-1}
c_w	0.000458	MPa^{-1}
ϕ_{edil}	0.0	degrees
η	3	MPa/(m/s)
$\sigma_{n,eref}$	200000000	MPa
$\sigma_{n,Eref}$	200000000	MPa

Table 4.2: Simulation parameters that were varied in the simulations

Parameter	**Value(s)**
k	1 mD, 10 μD, 100 nD
Tensile Strength, T_o	5 MPa, 12 MPa
Rate of propagation	5 cm/s, 1 mm/s

4.3 RESULTS AND DISCUSSION

4.3.1 Effect of rate of propagation

The effect of rate of propagation was investigated for both the high permeability (1 mD) case (Figure 4.3 and Figure 4.4) and the low permeability (100 nD) case (Figure 4.5 and Figure 4.6). For both cases, the value of K_I was higher for lower rates of propagation. This occurred because of the reduced poroelastic pressure response. The slowly propagating hydraulic fracture allows more time for fluid to flow into the incipient fracture than the rapidly propagating hydraulic fracture.

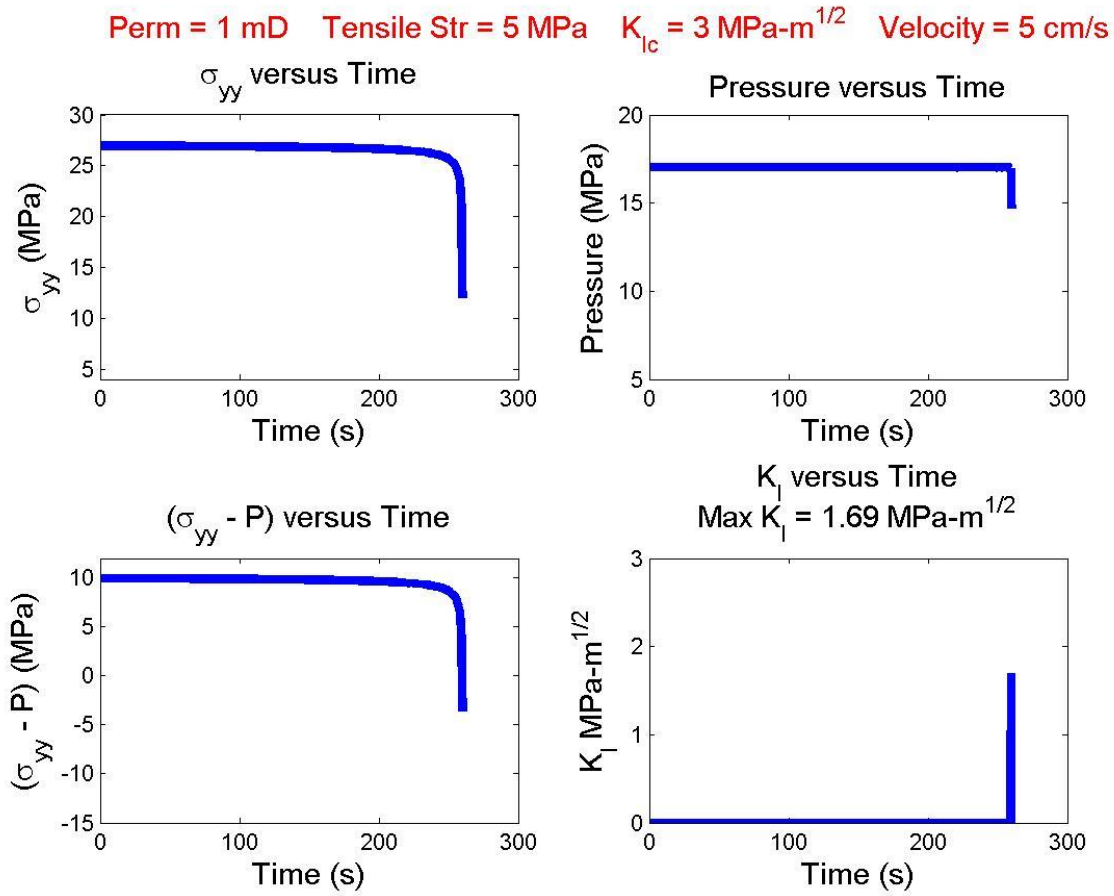

Figure 4.3: Pressure and K_I profiles of an opening fracture under varying σ_{yy} due to an approaching hydraulic fracture propagating with a velocity of 5 cm/s; matrix permeability of 1 mD, tensile strength of 5 MPa, and $K_{Ic}$of 3 MPa.m$^{1/2}$.

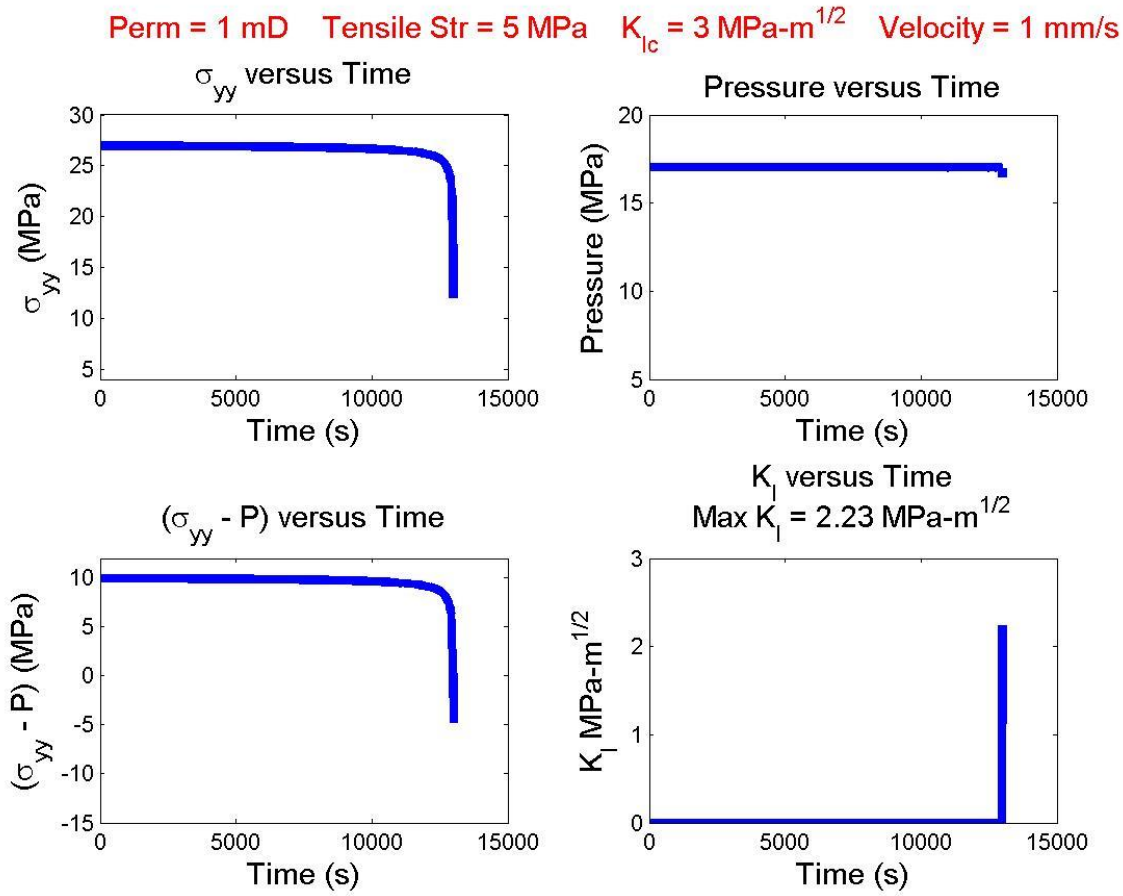

Figure 4.4: Pressure and K_I profiles of an opening fracture under varying σ_{yy} due to an approaching hydraulic fracture propagating with a velocity of 1 mm/s; matrix permeability of 1 mD, tensile strength of 5 MPa, and K_{Ic} of 3 MPa.m$^{1/2}$.

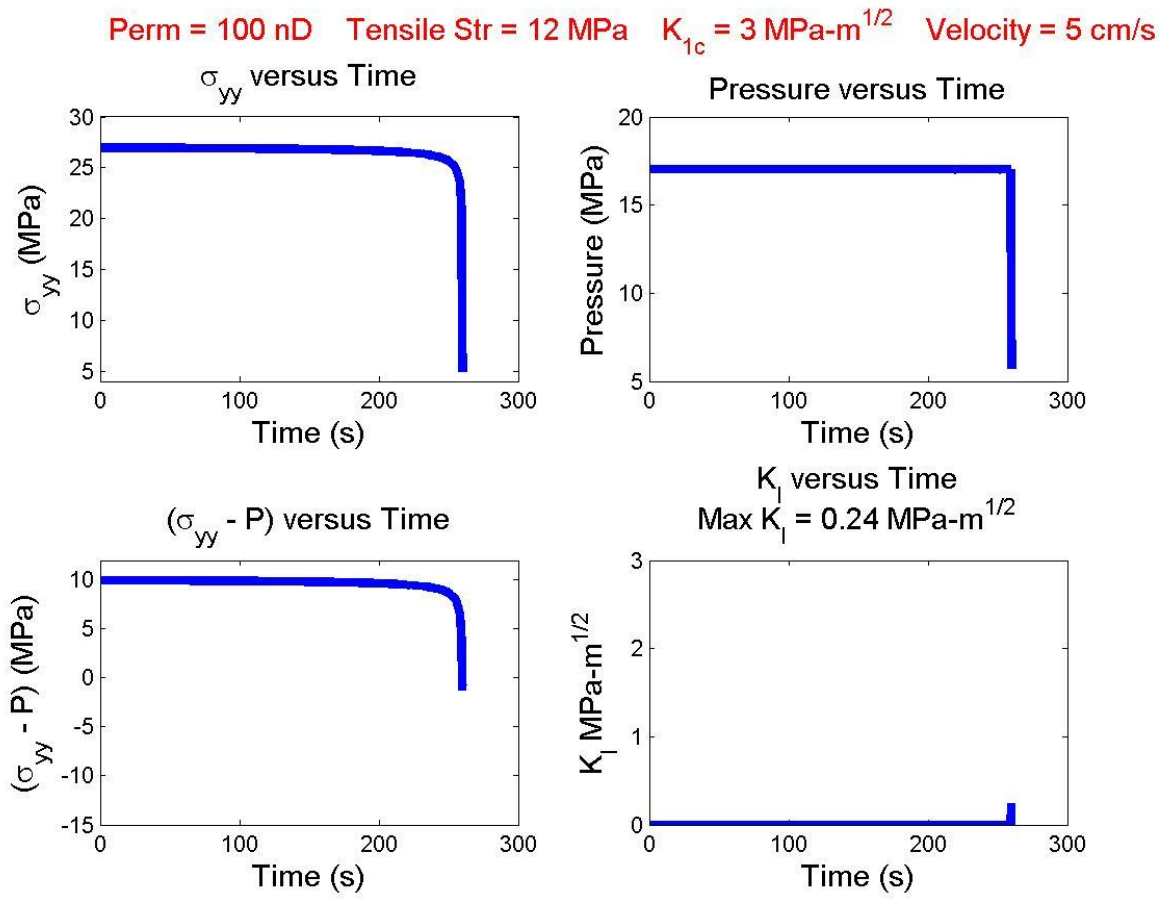

Figure 4.5: Pressure and K_I profiles of an opening fracture under varying σ_{yy} due to an approaching hydraulic fracture propagating with a velocity of 5 cm/s; matrix permeability of 100 nD, tensile strength of 12 MPa, and $K_{Ic}$of 3 MPa.m$^{1/2}$.

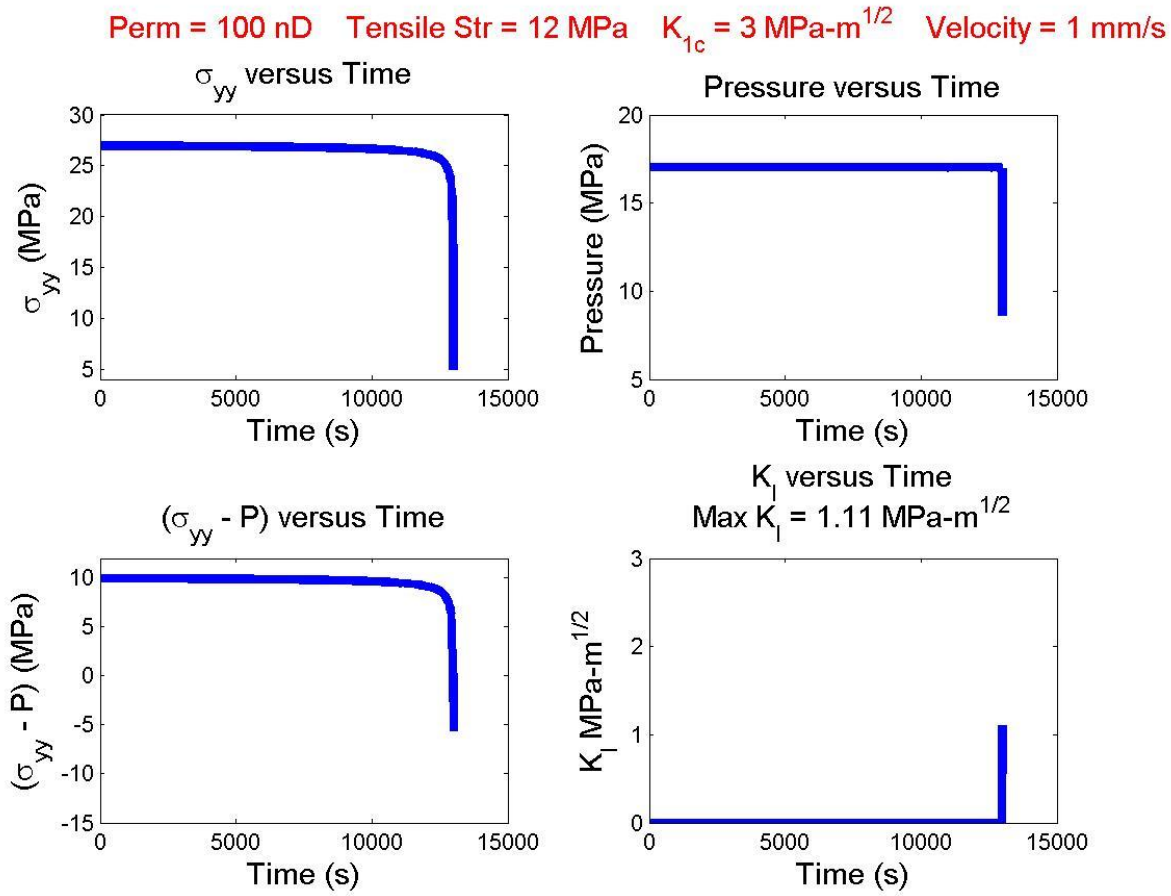

Figure 4.6: Pressure and K_I profiles of an opening fracture under varying σ_{yy} due to an approaching hydraulic fracture propagating with a velocity of 1 mm/s; matrix permeability of 100 nD, tensile strength of 12 MPa, and $K_{Ic}$of 3 MPa.m$^{1/2}$.

4.3.2 Effect of tensile yield strength

Figure 4.7 and Figure 4.8 show simulation results for two different values of tensile yield strength for 1 mD matrix permeability. Figure 4.9 and Figure 4.10, show results for two different values of tensile yield strength for 100 nD matrix permeability. K_I was greater for higher values of tensile yield strength.

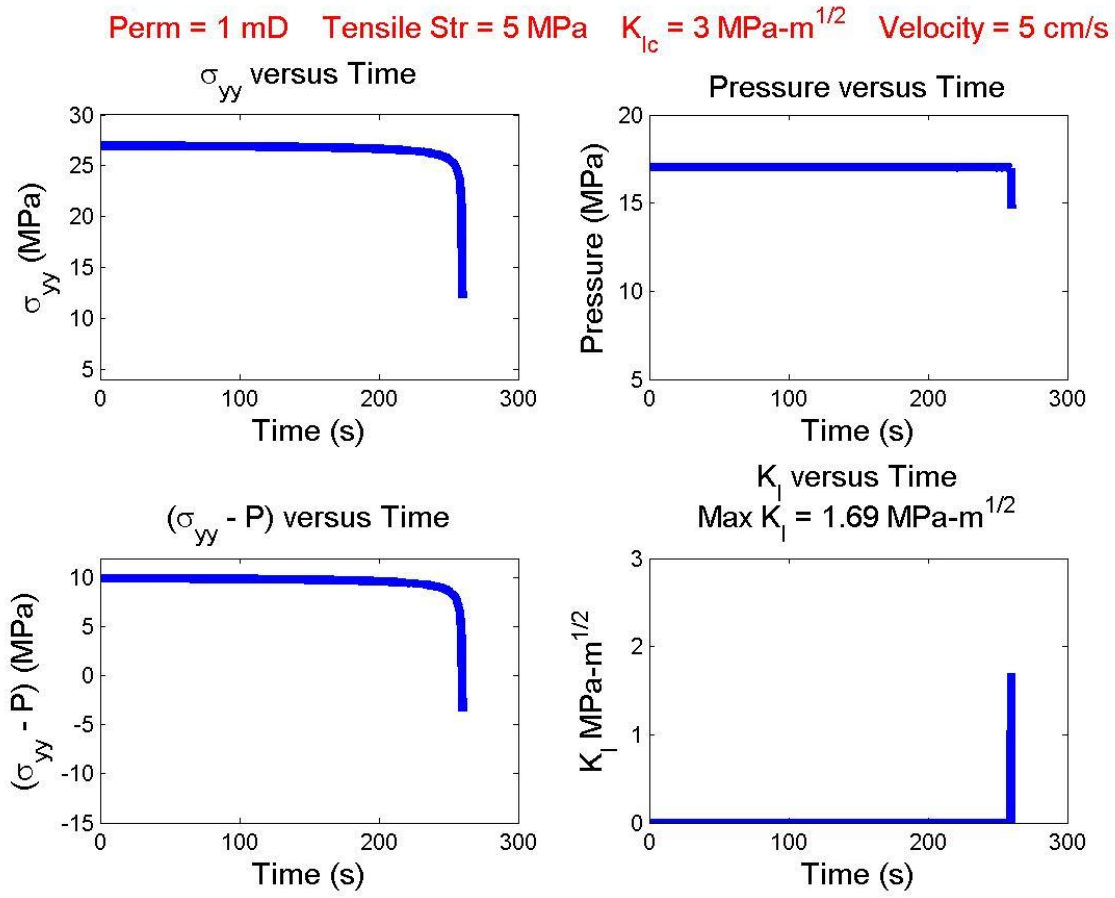

Figure 4.7: Pressure and K_I profiles of an opening fracture under varying σ_{yy} due to an approaching hydraulic fracture propagating with a velocity of 5 cm/s; matrix permeability of 1 mD, tensile strength of 5 MPa, and $K_{Ic}$of 3 MPa.m$^{1/2}$.

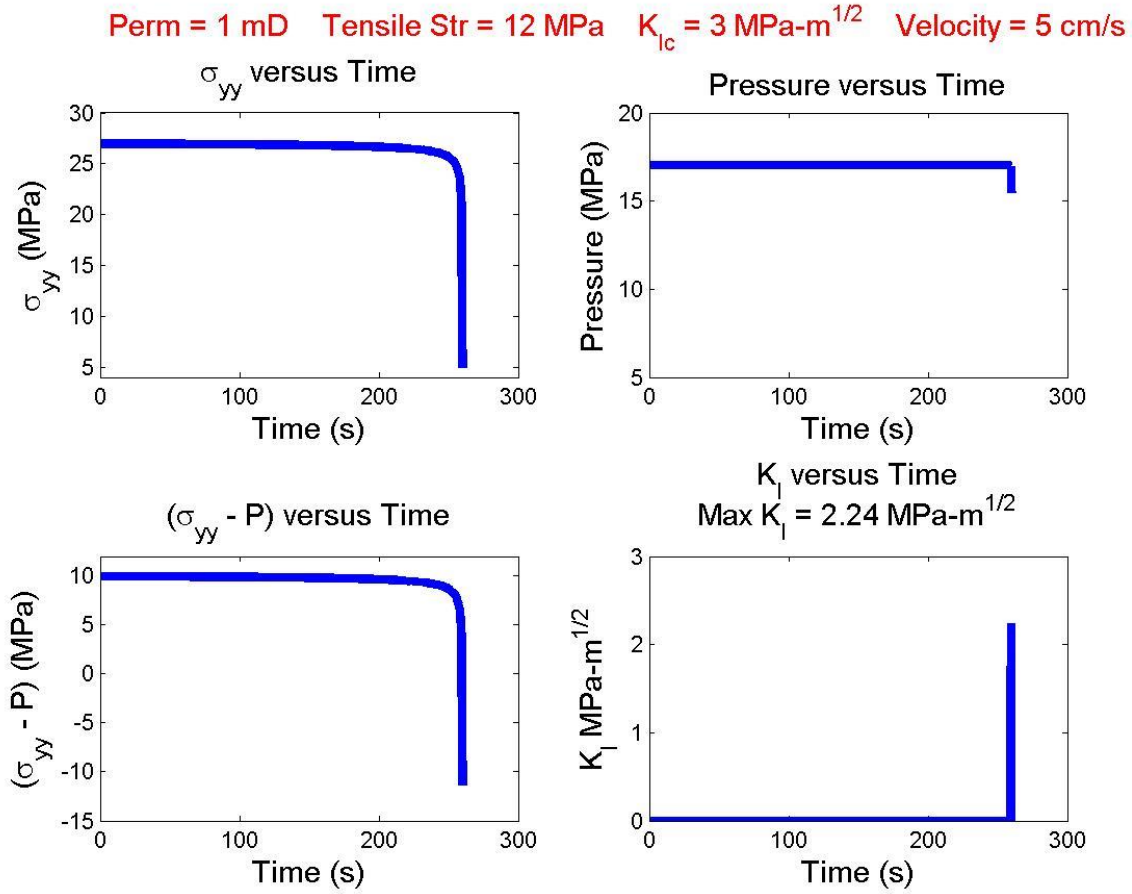

Figure 4.8: Pressure and K_I profiles of an opening incipient fracture under varying σ_{yy} due to an approaching hydraulic fracture propagating with a velocity of 5 cm/s; matrix permeability of 1 mD, tensile strength of 12 MPa, and $K_{Ic}$of 3 MPa.m$^{1/2}$.

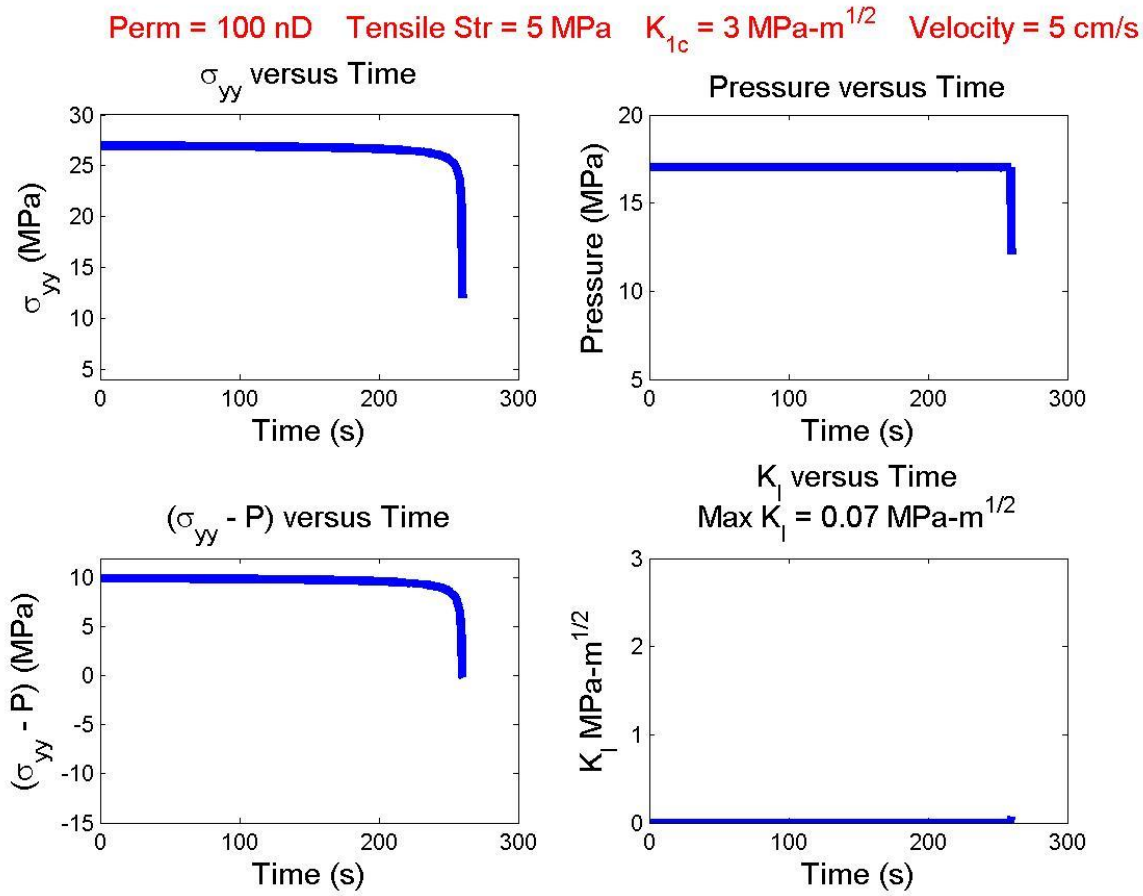

Figure 4.9: Pressure and K_I profiles of an opening fracture under varying σ_{yy} due to an approaching hydraulic fracture propagating with a velocity of 5 cm/s; matrix permeability of 100 nD, tensile strength of 5 MPa, and $K_{Ic}$of 3 MPa.m$^{1/2}$.

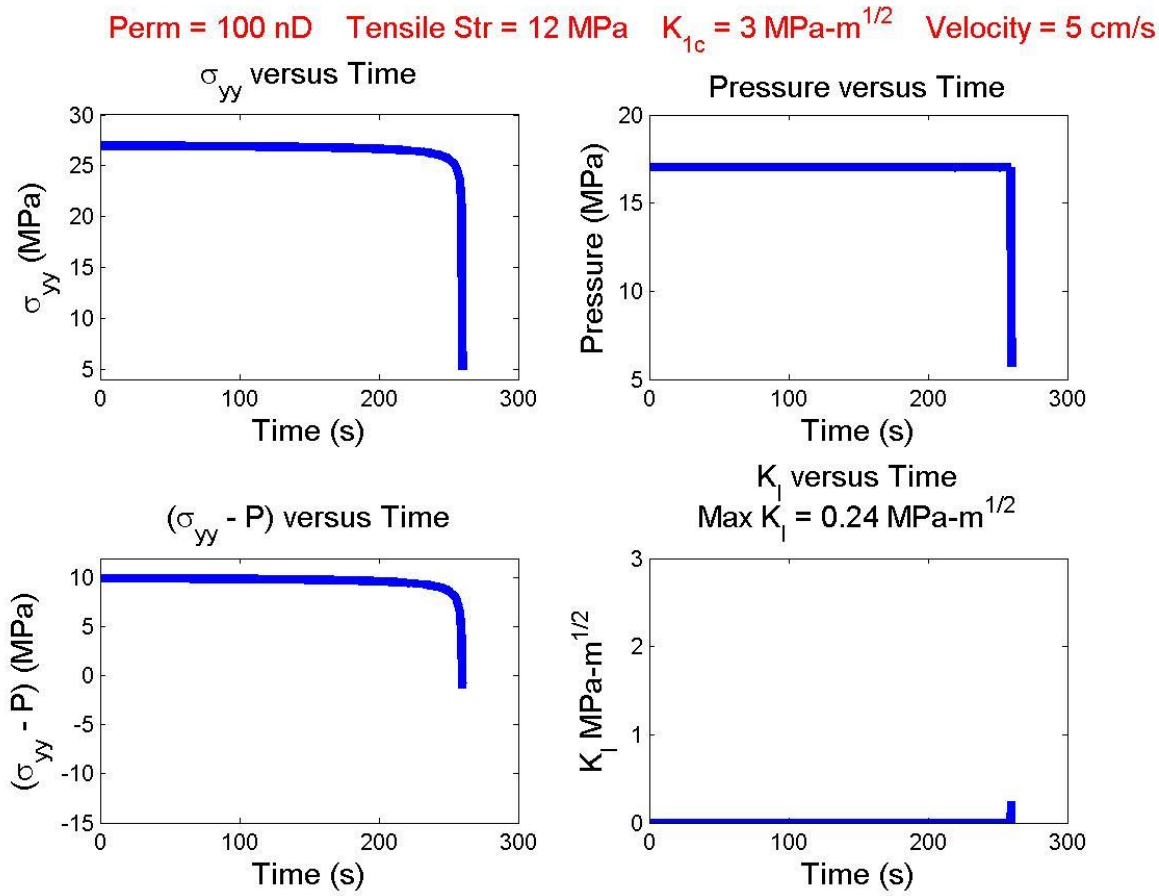

Figure 4.10: Pressure and K_I profiles of an opening fracture under varying σ_{yy} due to an approaching hydraulic fracture propagating with a velocity of 5 cm/s; matrix permeability of 100 nD, tensile strength of 12 MPa, and $K_{Ic}$of 3 MPa.m$^{1/2}$.

4.3.3 Effect of permeability

Two different combination of parameters (tensile strength, fracture toughness and rate of propagation) were used to evaluate the effect of permeability. In each case, permeability was increased from 1 mD to 100nD. Figure 4.8 and Figure 4.10 show the results for 1 mD and 100 nD respectively for the first set of parameters while Figure 4.11 and Figure 4.12 show the results for the second set of parameters. Lower values of K_I were observed for lower permeability values.

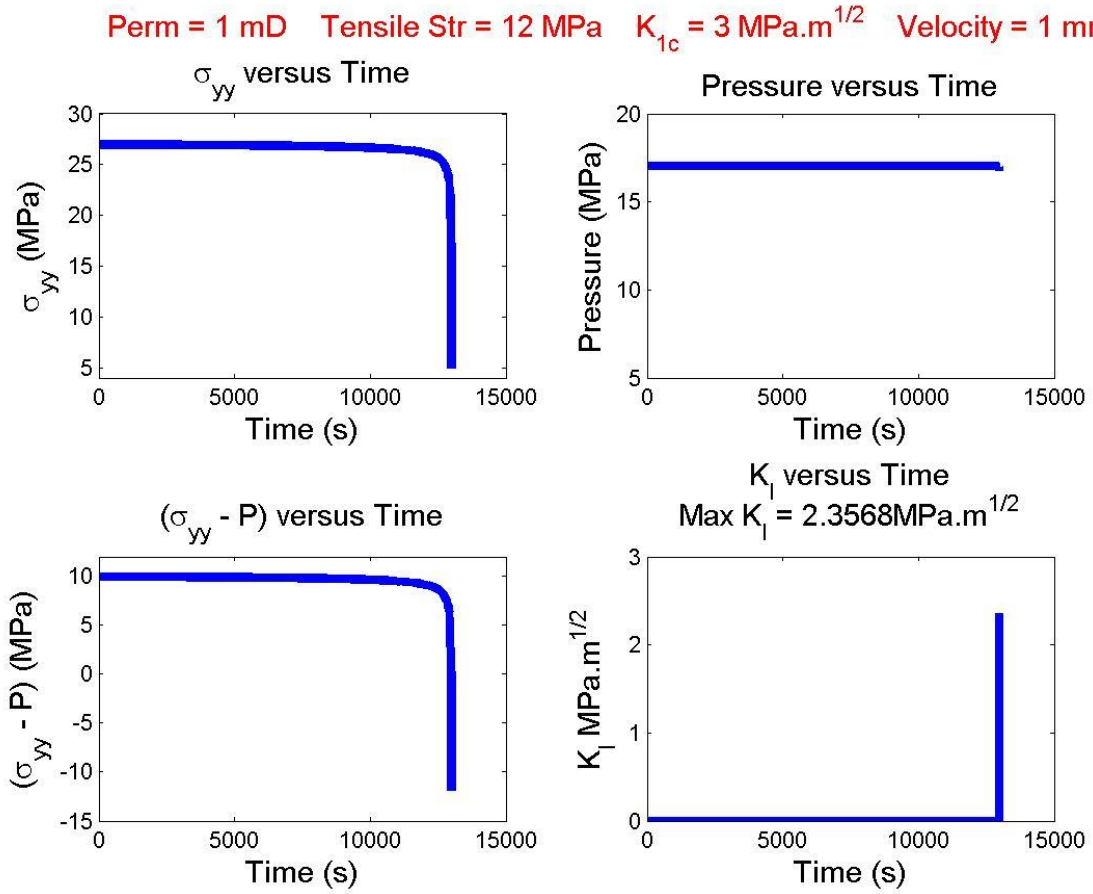

Figure 4.11: Pressure and K_I profiles of an opening fracture under varying σ_{yy} due to an approaching hydraulic fracture propagating with a velocity of 1 mm/s; matrix permeability of 1 mD, tensile strength of 12 MPa, and $K_{Ic}$of 3 MPa.m$^{1/2}$.

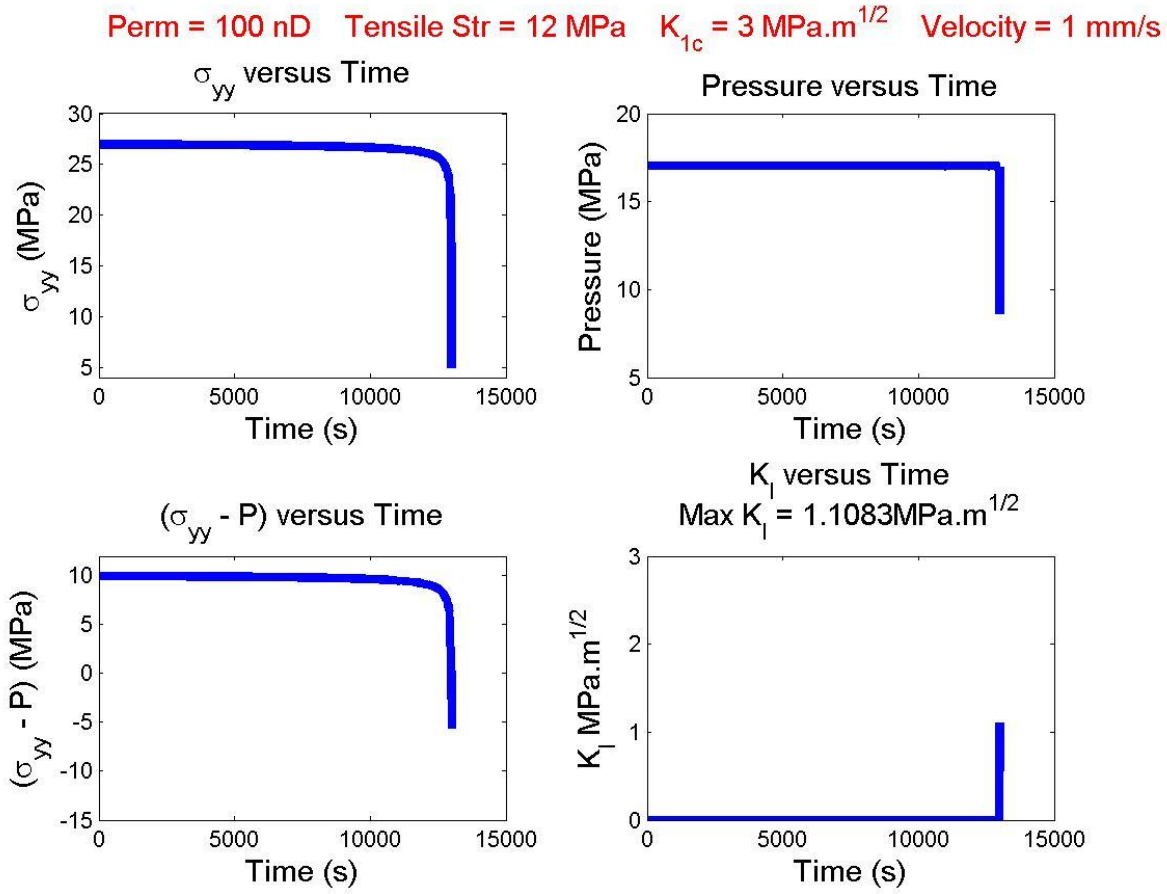

Figure 4.12: Pressure and K_I profiles of an opening fracture under varying σ_{yy} due to an approaching hydraulic fracture propagating with a velocity of 1 mm/s; matrix permeability of 100 nD, tensile strength of 12 MPa, and $K_{Ic}$of 3 MPa.m$^{1/2}$.

4.4 CONCLUSION

From the sensitivity study, the simulation conditions that gave the low values of K_I are low permeability, low tensile strength, and a high rate of propagation. The simulation conditions that resulted in the high values of K_I are high permeability, high tensile yield strength, and low rate of propagation.

Chapter 5 : Development of a Lost Circulation Mitigation Technique

5.1 INTRODUCTION

Previous chapters simulated the opening of the incipient fracture in order to determine the tendency for propagation under different conditions. This was necessary for the development of a crossing criterion because a low value of stress intensity factor (below the fracture toughness) suggests that the incipient fracture will not propagate, implying that termination will occur. These results were used to develop a crossing criterion. Once developed, the criterion was applied to test a proposed method for lost circulation mitigation.

5.2 METHODOLOGY

5.2.1 Slippage criterion

Renshaw and Pollard (1995) determined the stresses needed to prevent the slip of an interface at the instant of time when the stresses on the opposite end of the interface is high enough to re-initiate a new fracture using the equations for the stresses near a fracture tip based on linear elastic fracture mechanics. Gu and Weng (2010) extended the Renshaw and Pollard (1995) criterion to non-orthogonal intersections. This algorithm was implemented into CFRAC to determine whether the natural fracture will slip or response to an approaching hydraulic fracture.

Next, the Gu and Weng (2010) was extended to consider poroelastic effects. Our extended criterion is based on the idea that the fracture tip will blunt if reaches the natural fracture before incipient fractures have been able to initiate on the other side of the interface,

even if slippage has not yet occurred. The initiation of incipient fractures to reinitiate the fracture is time-dependent because these fractures cannot open unless fluid flows into them from the surrounding formation. Thus, we developed a criterion to predict whether incipient hydraulic fractures would have sufficient time to initiate prior to the arrival of the hydraulic fracture at the interface. If they do not, we assume that the fracture has terminated. At this point, fluid will likely begin to seep out from the hydraulic fracture into the natural fracture. The hydraulic fracture might propagate across the interface, regardless of this termination, but this process was not considered.

Significant simplifications are made in the development of this time-dependent crossing criterion. It is not intended to be quantitatively accurate but rather, it is intended to by hypothesis generation, demonstrate the possibility that matrix permeability could affect the tendency for fracture crossing and to qualitatively test how this process may be exploited for lost circulation mitigation.

5.2.2 Time dependent crossing criterion

The algorithm for the time dependent crossing criteria implemented into CFRAC is outlined below:

i. CFRAC estimates the net pressure of the approaching hydraulic fracture as well as the velocity of propagation.
ii. CFRAC performs a detailed numerical simulation of a hydraulic fracture approaching an interface at a constant rate of propagation by:

- Analytically calculating the induced stresses on the incipient fracture using eqn (4.7)
- Calculating the pressure in the incipient fracture using mass balance, the Vinsome and Westerveld (1980) leak-off model (in reverse, modeling leak-in), an elasticity solution relating fluid pressure to fracture volume
- Calculating the stress intensity factor of the incipient fracture at the moment when hydraulic fracture arrives and comparing it to a fracture toughness criterion

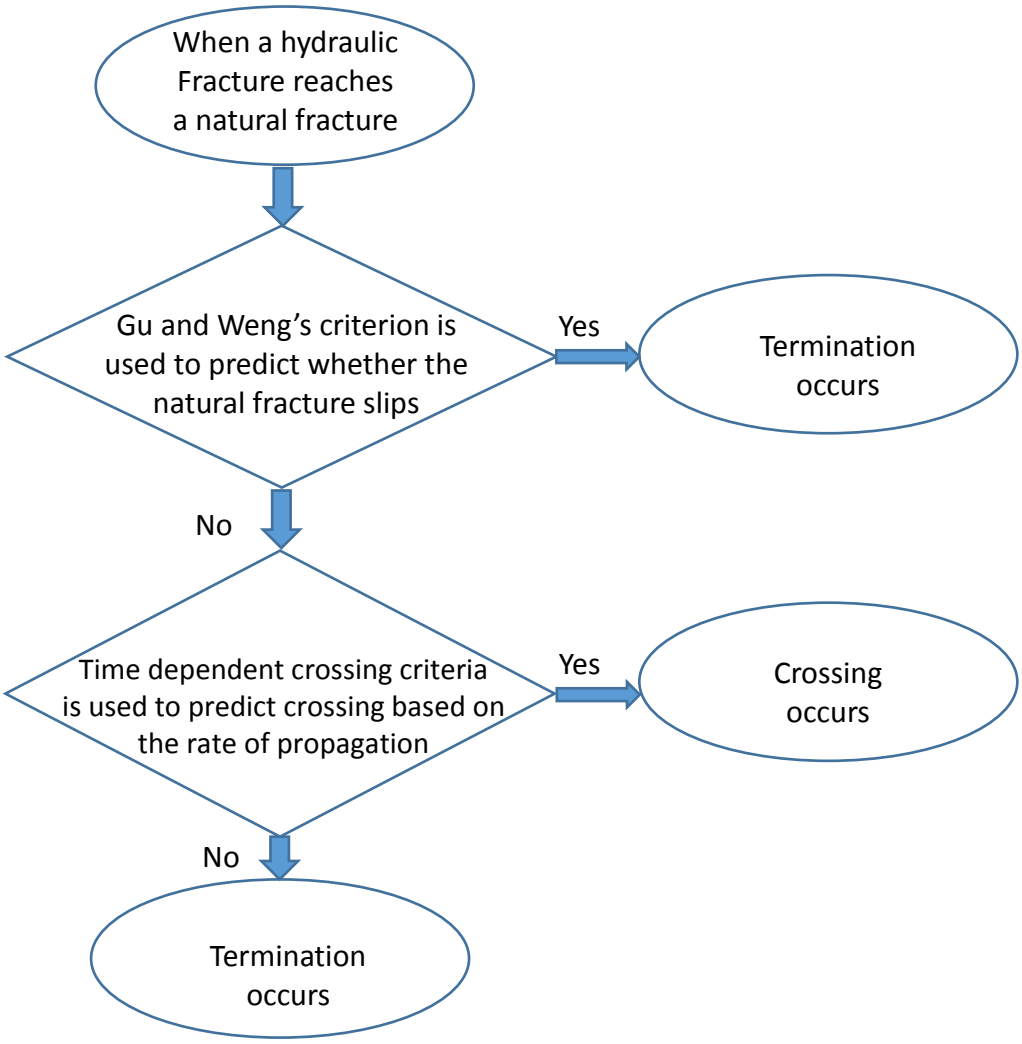

Figure 5.1: CFRAC simulation flow chat

5.2.3 Fracture network setup

Natural fractures do not usually align in the direction of the in-situ principal stresses, which implies that the angle of intersection between a hydraulic fracture and a natural fracture varies from 0 to 90°. Because the most favorable intersection angle for crossing is 90° (Blanton 1982), the fracture network was setup so that the hydraulic fractures intersected the natural fractures at 90° as shown in the figure below.

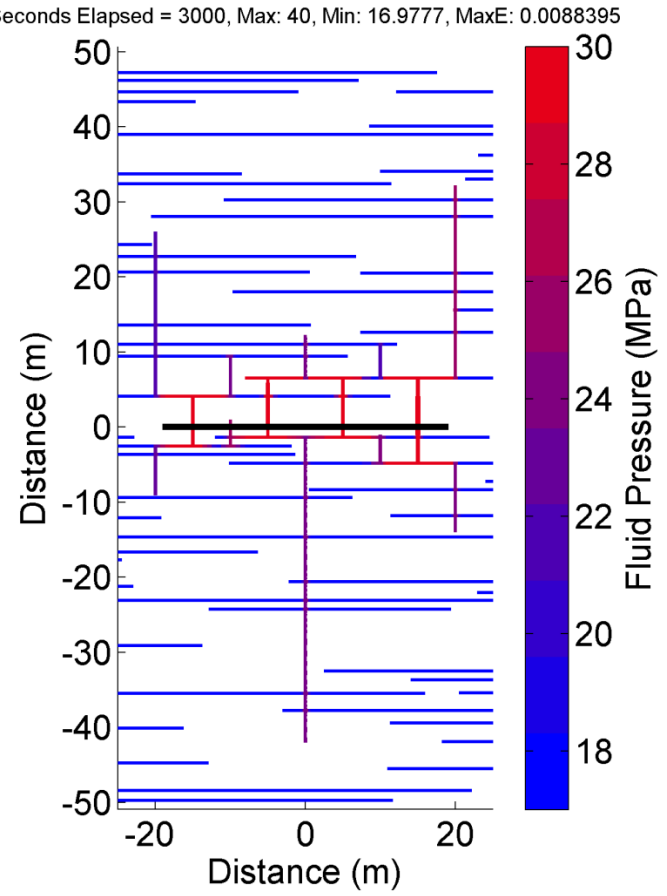

Figure 5.2: Map view of the fracture network showing the wellbore (black line) and the hydraulic fractures (parallel to the *y*-axis) intersecting the natural fractures (parallel to the *x*-axis)

5.2.2 LCM Technique

The sensitivity analysis in chapter 4 suggests that a slowly propagating hydraulic fracture will be more likely to cross a preexisting fracture (Figure 4.4). Knowledge of these processes in conjunction with the slippage and time dependent criteria implemented into CFRAC was used for the development of this novel technique in four sequential steps.

Firstly, a base lost circulation case, similar to lost circulation experienced during drilling, was set up in which the hydraulic fractures propagated continuously across the natural fractures without terminating. This was accomplished by injecting at a low rate.

The next step was to setup a simulation with high injection rate. This led to the formation of a complex fracture network. The initial hydraulic fractures terminated against the closest natural fractures. With continued injection, new hydraulic fractures initiated and also terminated against the next nearest natural fracture. This process was continued until a complex fracture network was produced.

Thirdly, a one-step LCM pumping sequence was tested. In sequence, injection was first performed at high rate to create a complex fracture network, as explained above. Second, the well was set at a constant pressure boundary condition, to simulate a drill onward scenario.

Finally a two-step LCM pumping sequence was tested. First, high rate injection of low fluid viscosity was performed to create a complex fracture network. Next, high viscosity fluid was pumped into the newly formed complex network. Finally, the well was placed at constant pressure to simulate a drill onward scenario.

5.2.3 Simulation Setup

Table 5.1: Simulation parameters that were held constant in all simulations

Parameter	**Value**	**Units**
σ_{yy}	40	MPa
σ_{xx}	27	MPa
σ_{xy}	0	MPa
P_{init}	17	MPa
k	10	µD
$Tensile\ yield\ strength$	12	MPa
G	15000	MPa
υ	0.25	unitless
h	100	m
μ	0.6	unitless
S_o	0.5	MPa
ϕ_{Edil}	0.0	degrees
ϕ_{edil}	2.5	degrees
A_{mat}	4	unitless
A_{frac}	4	unitless
$\sigma_{n,eref}$	10	MPa
$\sigma_{n,Eref}$	10	MPa
μ_f	1	cp
ϕ_i	0.03	unitless

Table 5.1: (Continued)

c_ϕ	0.00145	MPa^{-1}
c_w	0.000458	MPa^{-1}
e_0	0.0004	unitless
E_0	0.001	unitless

Table 5.2: Simulation parameters that varied in the simulations

Parameter	**Value(s)**
Maximum injection pressure	30 MPa, 50 MPa
Maximum injection flowrate	10 kg/s, 100 kg/s
Viscosity	Variable- either 1 cp fluid or 400 cp was used

5.3 RESULTS AND DISCUSSION

5.3.1 Base case – Lost circulation

Figure 5.3 shows that a hydraulic fracture from the well and continuously propagated through the formation. In this simulation, lost circulation has occurred. The natural fractures have not impeded the propagation of hydraulic fractures through the formation. Figure 5.4 shows

a plot of wellbore pressure and flow rate versus time. At a constant injection rate of 10 kg/s, circulation was lost at a wellbore pressure below 30 MPa.

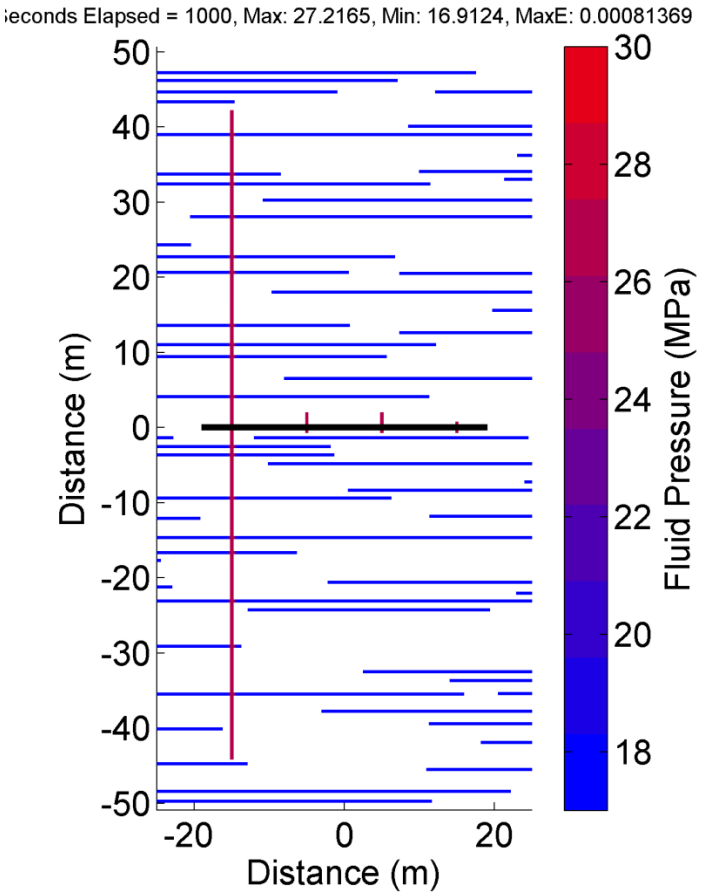

Figure 5.3: Map view of the fracture network at the end of the simulation. The black line is the well, the lines parallel to the y-axis are hydraulic fracture, and the lines parallel to the x-axis are natural fractures.

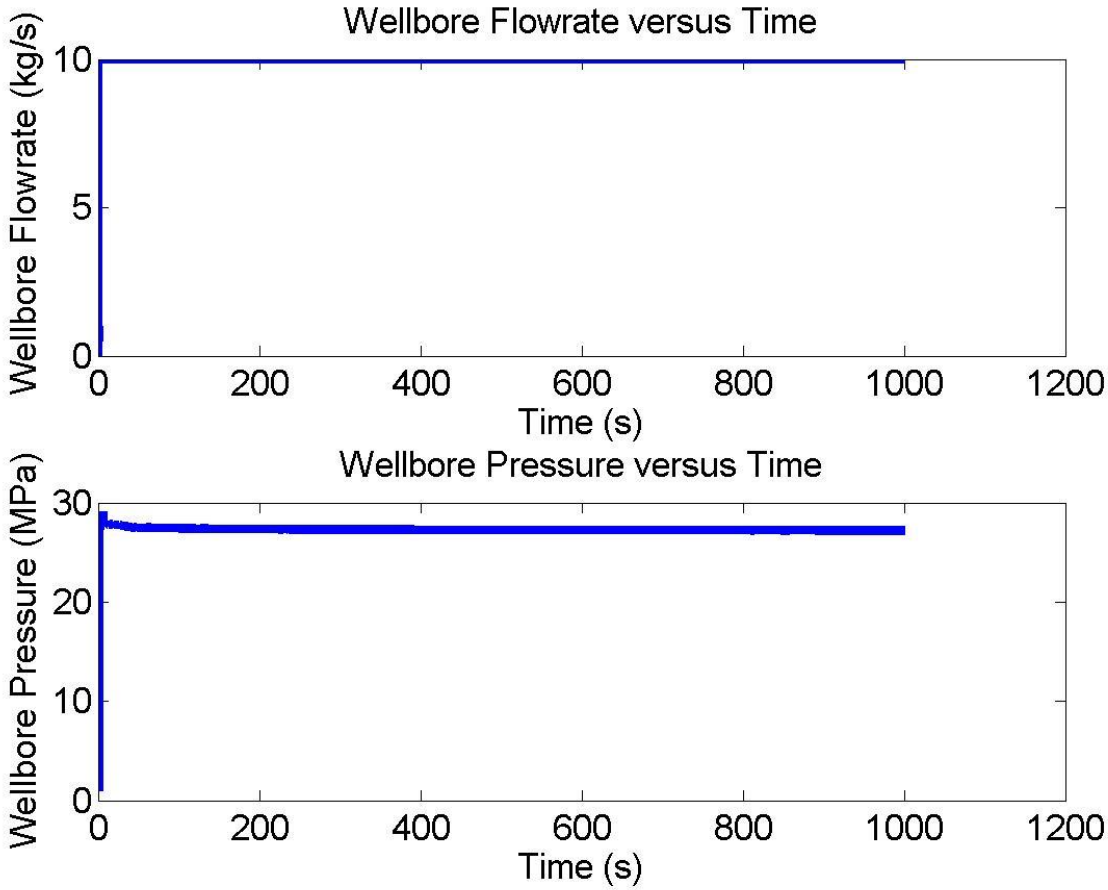

Figure 5.4: Plot of wellbore flowrate and wellbore pressure versus time for the lost circulation case

5.3.2 Stress cage effect due to complexity

Figure 5.5 shows the result of injection at 100 kg/s. At this rate, the hydraulic fractures tend to terminate against the natural fractures, creating a complex network. Figure 5.6 shows a plot of the wellbore pressure and flow rate versus time. Higher fluid pressure is required because the pressure must rise high enough to mechanically open the natural fractures that are oriented perpendicular to the maximum horizontal stress.

Figure 5.7 shows a contour plot of the change in σ_{xx} stress around the wellbore. The figure shows that the change in the normal stress is highest around the wellbore and decreases away from the wellbore. This increase in stress in the region of the wellbore effectively forms a stress cage.

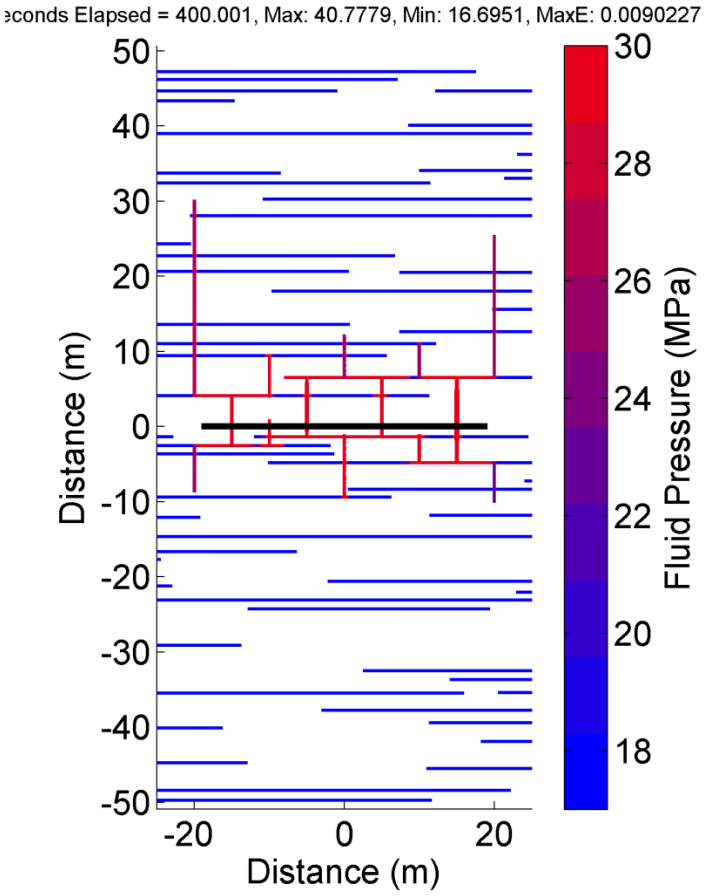

Figure 5.5: Map view of the fracture network at the end of the simulation. The black line is the well, the lines parallel to the y-axis are hydraulic fracture, and the lines parallel to the x-axis are natural fractures.

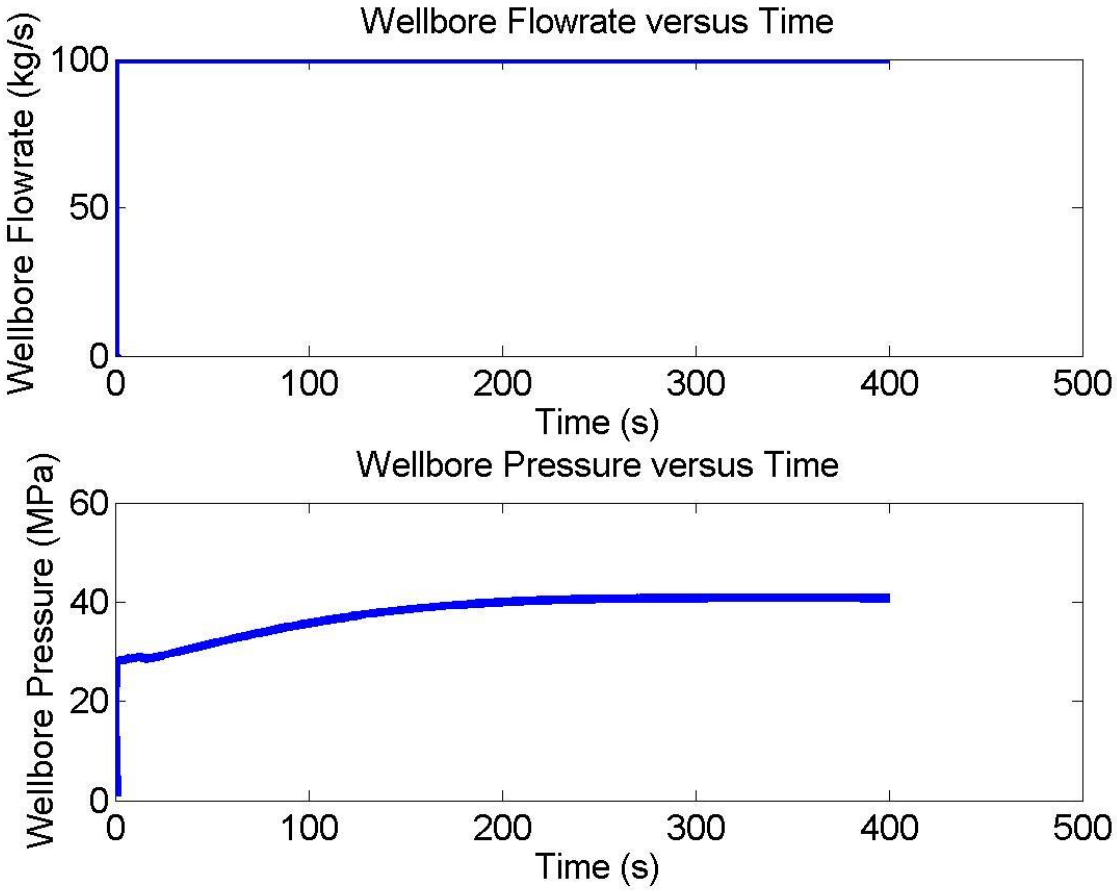

Figure 5.6: Plot of wellbore flowrate and wellbore pressure versus time

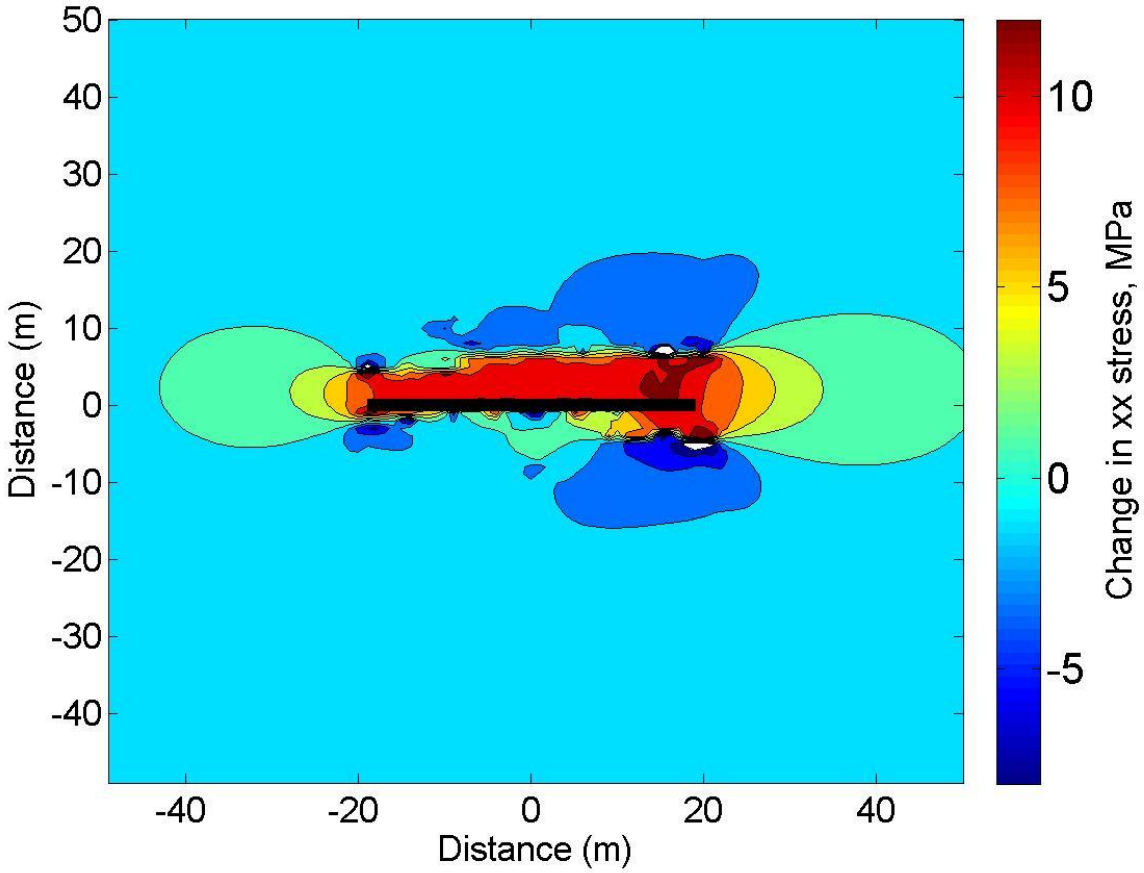

Figure 5.7: Contour plot of the change in the σ_{xx} stress

5.3.3 One-step LCM pumping sequence

In this sequence, a low viscosity fluid is injected at a high rate of 100 kg/s for 400 seconds to create the fracture complexity, and then a drill onward scenario is created by injecting fluid at a constant pressure until the end of the simulation. The movie of the simulation for this pumping sequence for the first 400 seconds is initially similar to the simulation from Section 5.3.2. However, when the drill onward period begins, the fracture network continues to grow (Figure 5.8).

The plot of wellbore flowrate in Figure 5.8 shows an increasing trend at constant maximum pressure of 40 MPa during the drill onward period. This is indicative of the continuous loss of fluid through the fracture network. The stress cage around the wellbore shown in Figure 5.9 prevented the initiation of new fractures because of the increased stress required for the initiation of new fractures. However it didn't prevent the further propagation of the existing fractures. This result indicates that the complex fracture network by itself was not able to mitigate lost circulation.

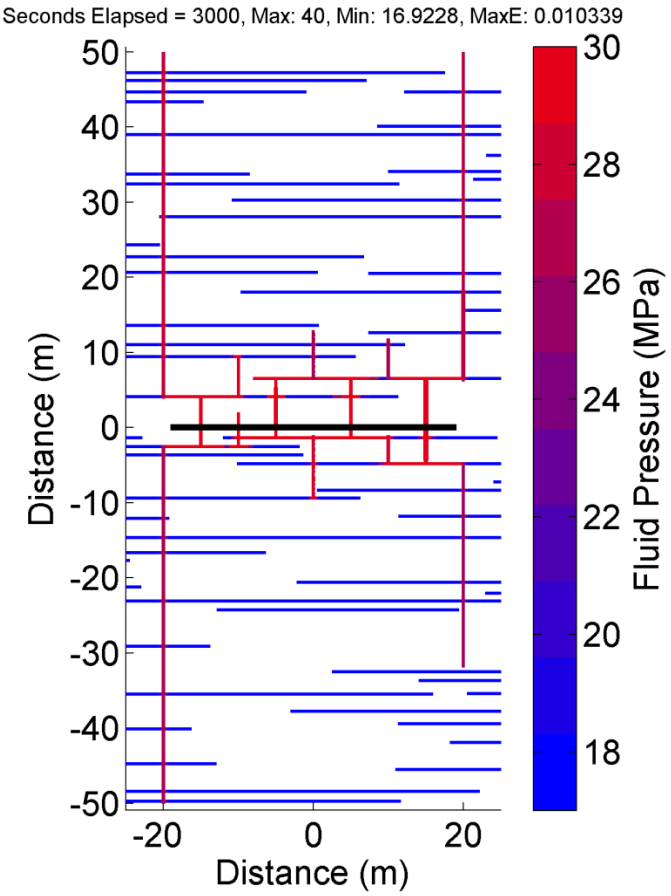

Figure 5.8: Map view of the fracture network at the end of the simulation. The black line is the well, the lines parallel to the y-axis are hydraulic fracture, and the lines parallel to the x-axis are natural fractures.

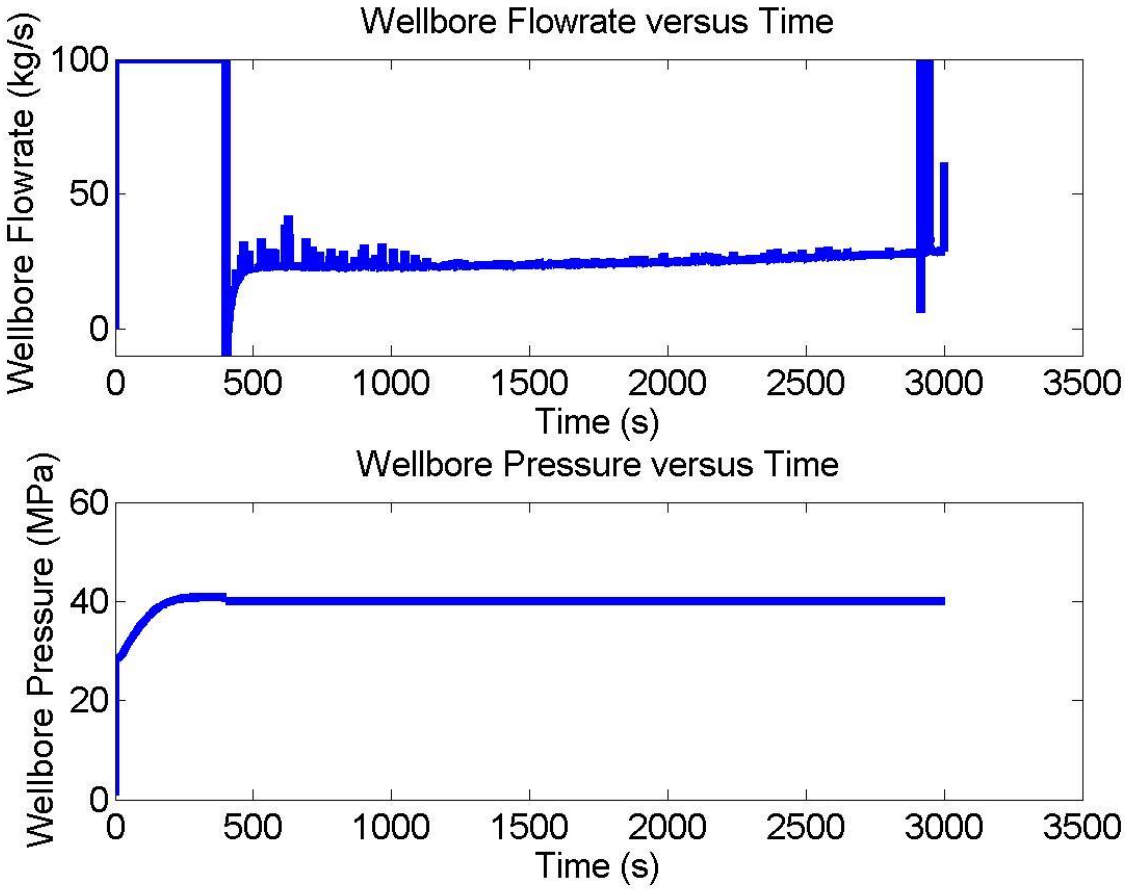

Figure 5.9: Plot of wellbore flowrate and wellbore pressure versus time

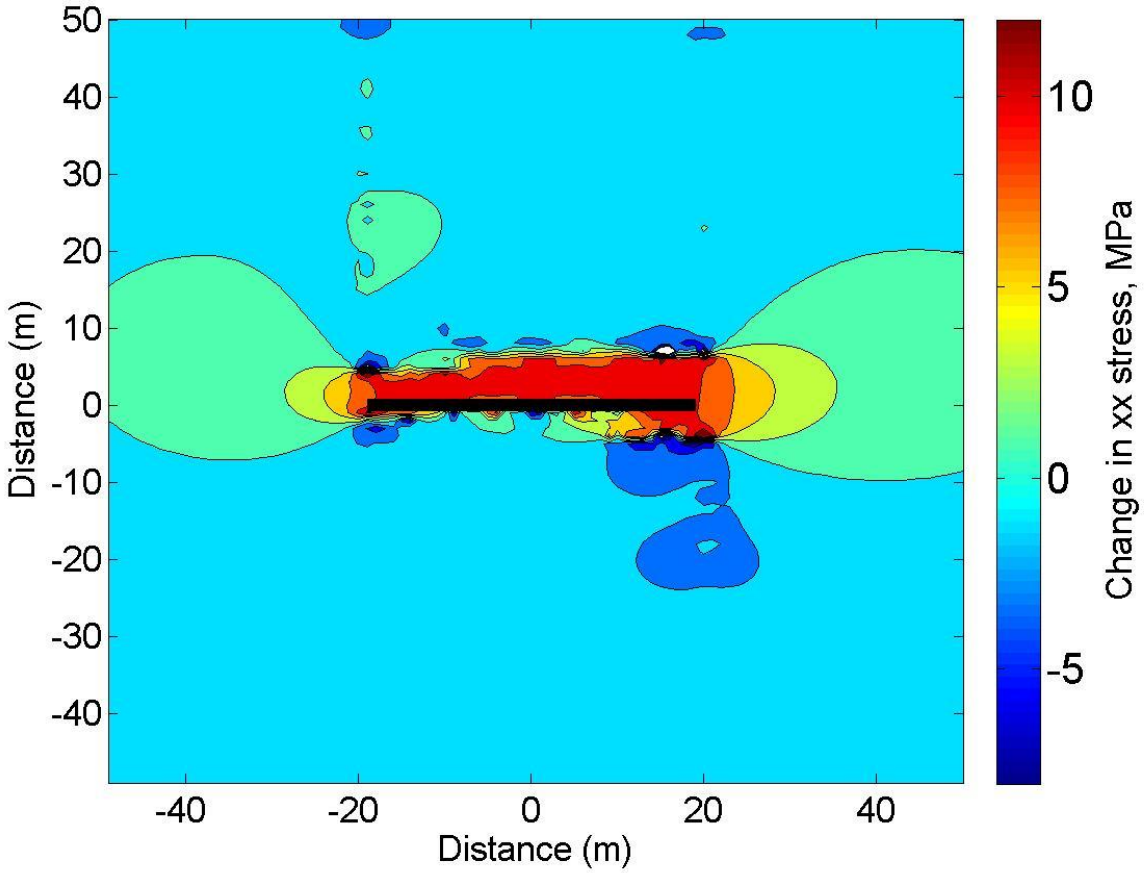

Figure 5.10: Contour plot of the change in σ_{xx} stress

5.3.4 Two-step LCM sequence

Because the one step LCM was not successful in mitigating the fluid loss, an extra step was added to the sequence. A low viscosity fluid was injected at a high rate for 400 seconds, followed by a high viscosity fluid at a low injection rate for another 600 seconds. Finally, a drill onward scenario at constant maximum pressure of 40 MPa was simulated.

Figure 5.11 shows that further propagation of the complex fracture network did not occur during the drill onward period. The difference can be seen by comparing Figure 5.8 and Figure

5.11. The high viscosity fluid pumped into the network plugged up the fractures, preventing any subsequent fluid from flowing into the network and causing fracture propagation.

In the figure above, the drill onward at a constant maximum pressure started from 1,000 seconds and afterwards the wellbore flow rate decreased continuously until the end of the simulation. This shows that while some loss of returns was occurring, this lost of returns was controlled and decreasing over time.

The stress contour plot in Figure 5.13 shows the stress cage effect around the wellbore.

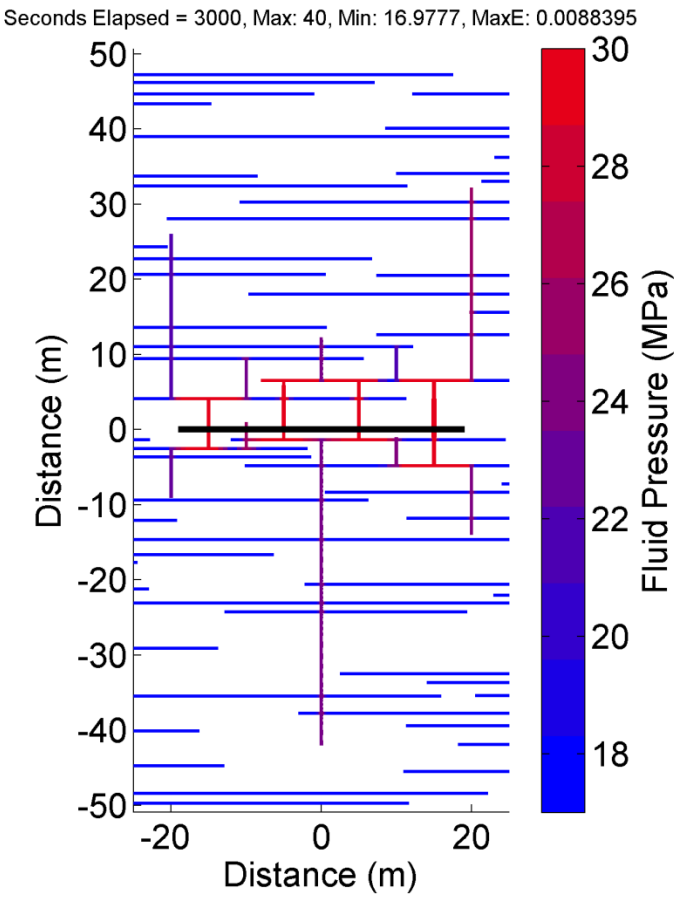

Figure 5.11: Map view of the fracture network at the end of the simulation. The black line is the well, the lines parallel to the y-axis are hydraulic fracture, and the lines parallel to the x-axis are natural fractures.

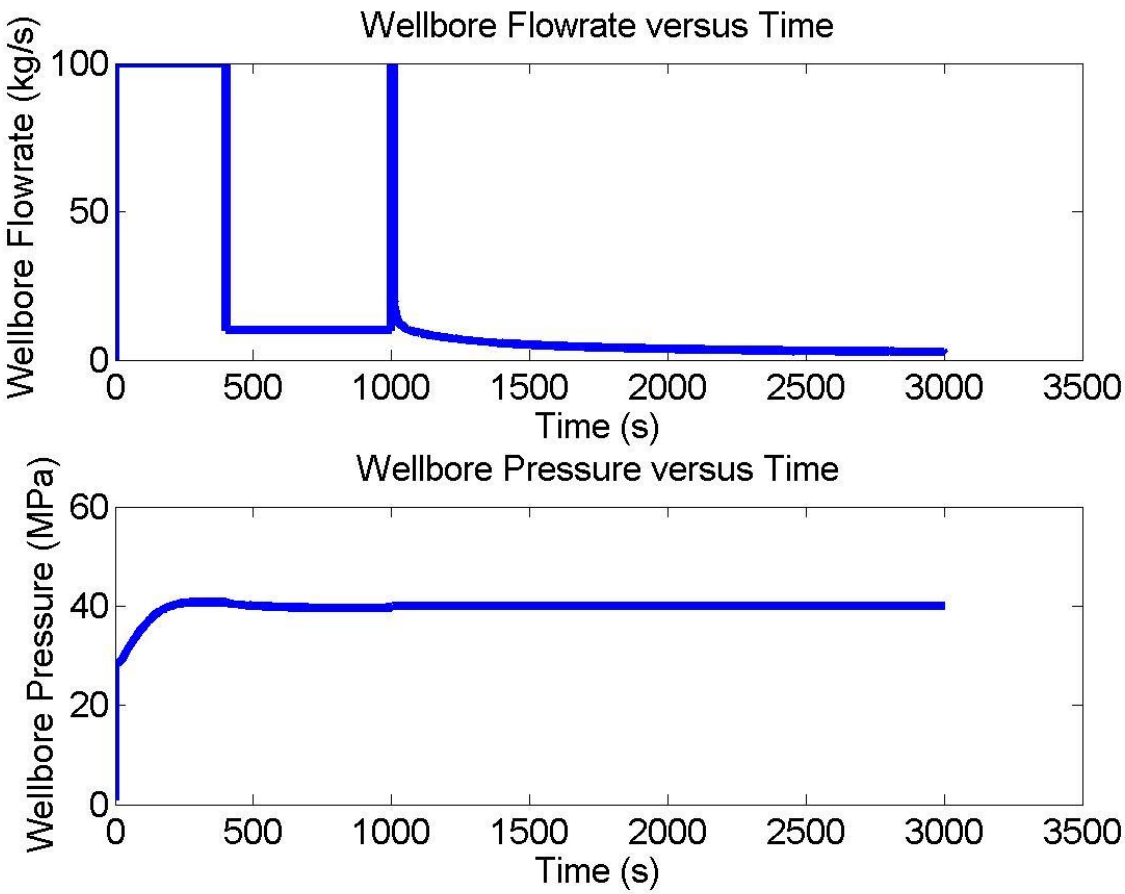

Figure 5.12: Plot of wellbore flowrate and wellbore pressure versus time

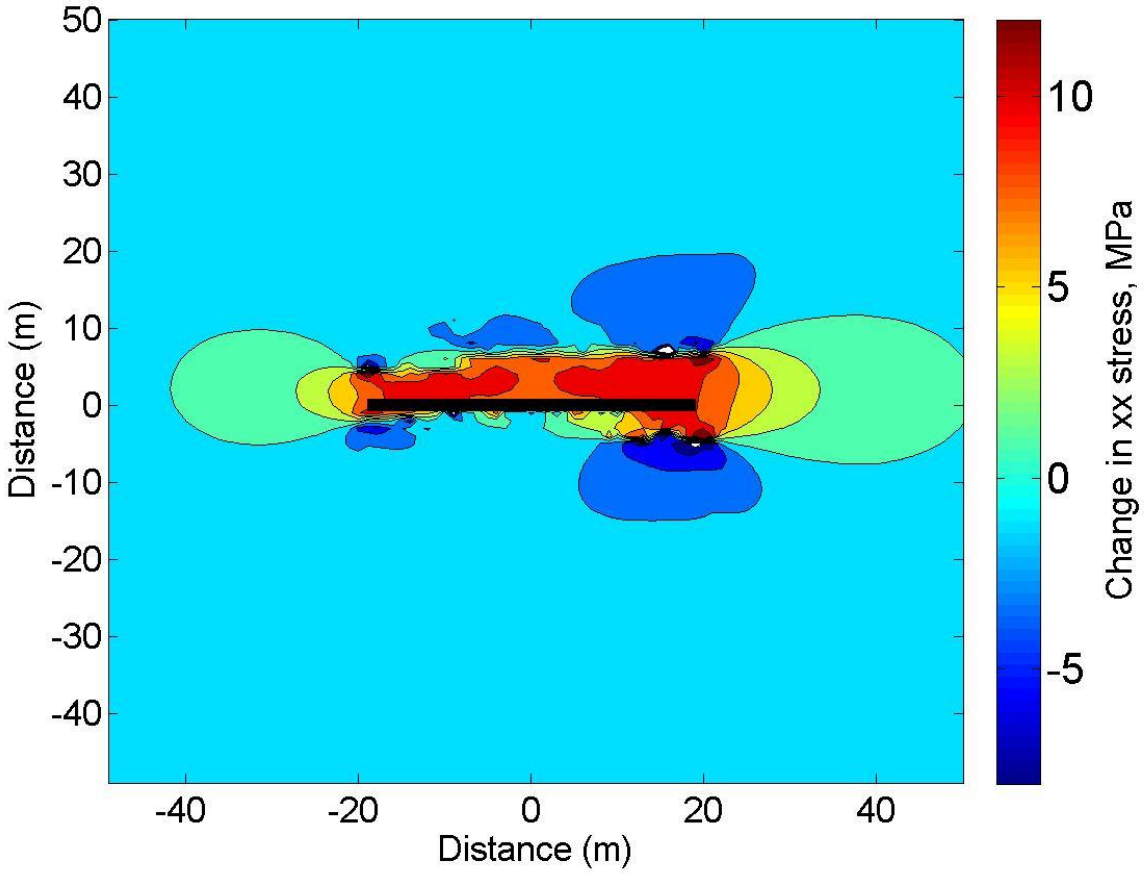

Figure 5.13: Contour plot of the change in σ_{xx} stress

5.4 CONCLUSION

Low rate of injection encourages crossing when a hydraulic fracture intersects a natural fracture. High rate of injection encourages termination and the formation of a complex fracture network. This increases the stresses around the wellbore, creating a stress cage

Pumping a two-step LCM sequence – high rate and low viscosity, followed by lower rate and high viscosity – may be able to create fracture propagation resistance by creating a complex network and a stress cage, and then plugging it up so flow through the network is difficult

Chapter 6 : Conclusions

A novel hypothesis for how a time-dependent poroelastic effect may encourage fracture termination was developed and tested. The results suggest that with sufficiently low permeability, it may require minutes or more for incipient fractures to initiate on the opposite side of the natural fracture. During this time, the propagating hydraulic fracture may be able to cause slip and prevent the incipient fractures from fully forming and allowing crossing. Or, the propagating fracture may reach the natural fracture, blunting the crack tip. This suggests crossing may be more likely to occur in low permeability formations and when the fracture is propagating rapidly.

This insight was used to develop a semi-analytical time-dependent crossing criterion. The criterion is not expected to be quantitatively accurate, but it qualitatively reflects our hypothesized mechanism for how propagation may occur. This criterion was applied to test a novel lost circulation mitigation procedure for low permeability formations. The results revealed that:

- Injecting fluid at high rate creates a complex fracture network and increases the stresses around the wellbore, creating a stress cage
- Pumping a two-step sequence of high injection rate and low fluid viscosity, followed by high viscosity fluid may be able to create fracture propagation resistance and reduce lost circulation. The process creates a complex fracture network and stress cage with the initial injection, and then plugs the complex fracture network with the second injection.

This proposed mechanism could be used to proactively prevent lost circulation, but not to mitigate lost circulation that has already occurred. In practice, it could be useful to perform this

type of proactive wellbore strengthening if mud weight increase is planned due to drilling through an overpressured formation.

It may also be possible to apply these concepts to hydraulic fracture design. Fracture complexity can be desirable or desirable for hydraulic fracturing. Either way, it would be useful to be able to control the development of complexity in the reservoir.

Further work is needed to test the hypothesized mechanisms. Experimental work is needed to validate/investigate the proposed time-dependent crossing criterion and the two-step LCM pumping sequence.

Nomenclature

E: Void aperture, mm

E_0: Reference void aperture, mm

e: Hydraulic aperture, mm

e_0: Reference hydraulic aperture, mm

G: Shear modulus, GPa

h: Out of plane fracture width, or height, m

K_I: Stress intensity factor, MPa-$m^{1/2}$

K_{Ic}: Fracture toughness, MPa-$m^{1/2}$

k: Permeability, m^2

P_{init}: Initial formation fluid pressure, MPa

F_{fm}: Mass rate of leakoff, kg/(s- m^2)

S_o: Cohesion, MPa

s_f and s_m: Mass source term per area, kg/(s-m^2) and kg/(s-m^3)

T: Transmissivity, m^3

μ: Coefficient of friction, unitless

ρ: Density, kg/m^3

σ_n, $\sigma_{\beta y}$: Normal stress, MPa

σ_{yy}: Remote compressive stress in the y direction, MPa

σ_{xx}: Remote compressive stress in the x direction, MPa

τ, τ_β: Shear stress, MPa

υ: Poisson's ratio, unitless

$\sigma_{n,Eref}$: Stress that causes 90% decrease in the void fracture aperture, MPa

$\sigma_{n,eref}$: Stress that causes 90% decrease in the hydraulic fracture aperture, MPa

ϕ_{Edil}: Shear dilation angle void aperture, ^{o}

ϕ_{edil}: Shear dilation angle hydraulic aperture, ^{o}

σ'_{xx}: Terzaghi effective maximum principal stress, MPa

σ'_{yy}: Terzaghi effective minimum principal stress, MPa

T_o: Tensile strength, MPa

t: Time, s

x: Distance, m

ϕ: Porosity, unitless

D_s: Cumulative sliding displacement, m

E_{open}: Mechanical opening, mm

σ'_n: Effective normal stress, MPa

η: Radiation damping coefficient, MPa/(m/s)

a: Fracture half-length, m

P_{net}: Net pressure, MPa

C_p: Polymer concentration, ppm

μ_{app}: Apparent viscosity, Pa-s

μ_w: Water viscosity, Pa-s

μ_p^0: Zero shear rate viscosity, Pa-s

A_{mat} and A_{frac}: Linear coefficients for matrix and fracture flow, unitless

$\dot{\gamma}_{eff}$: Apparent shear rate, s^{-1}

v: Velocity, m/s

r_i: Distance, m

L_{f_c}: Incipient fracture half length, m

L_{f_i}: Initial hydraulic fracture half length, m

$\sigma_{yy}{}^r$: Remote compressive stress in the y direction, MPa

ϕ_i: Initial matrix porosity, unitless

c_ϕ: Matrix porosity compressibility, MPa^{-1}

c_w: Fluid Compressibility, MPa^{-1}

References

Aston, M. S., Alberty, M. W., McLean, M. R., De Jong, H. J., and Armagost, K. 2004. Drilling Fluids for Wellbore Strengthening. *Society of Petroleum Engineers*. doi:10.2118/87130-MS.

Bahorich, B., Olson, J. E., and Holder, J. 2012. Examining the Effect of Cemented Natural Fractures on Hydraulic Fracture Propagation in Hydrostone Block Experiments. *Society of Petroleum Engineers*. doi:10.2118/160197-MS

Barton, N., S. Bandis, K. Bakhtar. 1985. Strength, deformation and conductivity coupling of rock joints. *International Journal of Rock Mechanics and Mining Sciences and Geomechanics* Abstracts 22 (3): 121-140, doi: 10.1016/0148-9062(85)93227-9.

Blanton, T. 1982. An experimental study of interaction between hydraulically induced and pre-existing fractures. *SPE 10847. Paper presented at the SPE Unconventional Gas Recovery Symposium*, Pittsburgh, Pennsylvania, doi:10.2118/10847-MS.

Carreau, P. J. 1972. Rheology equations from molecular network theories. *Transactions of the Society of Rheology* 16 (1): 99-127, doi: 10.1122/1.549276.

Chilingarian, V. G., Vorabutr, P. 1983. Drilling and drilling fluids, Elsevier Scientific Company.

Chuprakov, D. A., Akulich, A. V., Siebrits, E., and Thiercelin, M. 2011. Hydraulic-Fracture Propagation in a Naturally Fractured Reservoir. *Society of Petroleum Engineers*. doi:10.2118/128715-PA.

Chuprakov, D., Melchaeva, O., and Prioul, R. 2013. Hydraulic Fracture Propagation Across a Weak Discontinuity Controlled by Fluid Injection. *International Society for Rock Mechanics*.

Chuprakov, D. A., and Prioul, R. 2015. Hydraulic Fracture Height Containment by Weak Horizontal Interfaces. *Society of Petroleum Engineers*. doi:10.2118/173337-MS

Dahi-Taleghani, A., and Olson, J. E. 2011. Numerical Modeling of Multistranded -Hydraulic-Fracture Propagation: Accounting for the Interaction Between Induced and Natural Fractures. *Society of Petroleum Engineers*. doi:10.2118/124884-PA.

Delshad, M., Kim D. H., Adedeji O. A., Huh C., Pope G. A., Tarahhom F. 2008. Mechanistic interpretation and utilization of viscoelastic behavior of polymer solutions for improved polymer-flood efficiency. *Paper SPE 113620 presented at the SPE Symposium on Improved Oil Recovery*, Tulsa, OK, doi: 10.2118/113620-MS.

Dupriest, F. E. 2005. Fracture Closure Stress (FCS) and Lost Returns Practices. *Society of Petroleum Engineers*. doi:10.2118/92192-MS.

Gu, H., and Weng X. 2010. Criterion for fractures crossing frictional interfaces at non-orthogonal angles. ARMA 10-198. *Paper presented at the 44th U.S. Rock Mechanics Symposium and 5th U.S.-Canada Rock Mechanics Symposium*, Salt Lake City, Utah. 135.

Gu, H., Weng, X., Lund, J. B., Mack, M. G., Ganguly, U., & Suarez-Rivera, R. 2011. Hydraulic Fracture Crossing Natural Fracture at Non-Orthogonal Angles, A Criterion, Its Validation and Applications. *Society of Petroleum Engineers*. doi:10.2118/139984-MS.

He M., Evans A. G., Hutchinnson J. W. 1989. Crack deflection at an interface between dissimilar elastic materials. *International Journal of Solids and Structure* doi:10.1016/0020-7683(94)90025-6.

Helgeson, D. E., Aydin A. 1991. Characteristics of joint propagation across layer interfaces in sedimentary rocks, Journal of Structural Geology, Volume 13, Issue 8, 1991, Pages 897-911, ISSN 0191-8141, http://dx.doi.org/10.1016/0191-8141(91)90085-W.

Heuze, F. E., Shaffer R. J., Ingraffea A. R., and Nilson R. H. 1990. Propagation of fluid-driven fractures in jointed rock. Part 1 - development and validation of methods of analysis. *International Journal of Rock Mechanics and Mining Sciences and Geomechanics*, Abstracts, 27(4), 243-254, doi:10.1016/0148-9062(90)90527-9.

Howard, G. C., and Fast, C. R. 1957. Optimum Fluid Characteristics for Fracture Extension. *American Petroleum Institute.*

Howard, G. C., and Scott, P. P. 1951. An Analysis and the Control of Lost Circulation. *Society of Petroleum Engineers*. doi:10.2118/951171-G.

Ivan, C., Bruton, J., and Bloys, B. 2003. How can we best manage lost circulation? AADE-03-NTCE-38, *AADE National Technology Conference Practical Solutions for Drilling Challenges*, Houston, Texas.

Ma, Y., McClure, M. W., 2015. Diagnosis of Induced Hydraulic Fractures during Polymer Injection. Masters Report, University of Texas at Austin.

McClure, M. W. 2012. Modeling and characterization of hydraulic stimulation and induced seismicity in geothermal and shale gas reservoirs. PhD dissertation, Stanford University, Stanford, California.

Morita, N., Black, A. D., and Guh, G.-F. 1990. Theory of Lost Circulation Pressure. *Society of Petroleum Engineers*. doi:10.2118/20409-MS.

Murchison, W. J 2006. Lost Circulation for the Man on the Rig. Murchison Drilling Schools, Inc.

Pollard, D.D. and Segall, P. 1987. Theoretical Displacements and Stresses near Fractures in Rock: With Applications to Faults, Joints, Veins, Dikes, and Solution Surfaces, in Fracture Mechanics of Rock, B.K. Atkinson, ed. London: Academic Press.

Renshaw, C. E., and Pollard D. D. 1995. An experimentally verified criterion for propagation across unbounded frictional interfaces in brittle, linear elastic materials. *International Journal of Rock Mechanics and Mining Sciences and Geomechanics* Abstracts, 32(3), 237-249, doi:10.1016/0148-9062(94)00037-4.

Segall, P. 2010. Earthquake and Volcano Deformation, Princeton University Press, Princeton, N.J.

Shewchuk, Jonathan Richard. 1996. Triangle: Engineering a 2D Quality Mesh Generator and Delaunay Triangulator. *Lecture Notes in Computer Science* **1148**: 203-222.

Shou, K. J., S. L. Crouch. 1995. A higher order displacement discontinuity method for analysis of crack problems. *International Journal of Rock Mechanics and Mining Sciences and Geomechanics* Abstracts 32 (1): 49-55, doi: 10.1016/0148-9062(94)00016-V.

Thiercelin, M., and Makkhyu, E. 2007. Stress Field In the Vicinity of a Natural Fault Activated By the Propagation of an Induced Hydraulic Fracture. *American Rock Mechanics Association*.

Thiercelin, M. 2009. Hydraulic fracture propagation in discontinuous media. *Presented at the international conference of Rock Joints and Jointed Rock Masses*, Tucson, Arizona.

Van Oort, E., Friedheim, J. E., Pierce, T., & Lee, J. 2009. Avoiding Losses in Depleted and Weak Zones by Constantly Strengthening Wellbores. *Society of Petroleum Engineers*. doi:10.2118/125093-PA.

Vinsome, P. K. W., and Westerveld, J. 1980. A Simple Method For Predicting Cap And Base Rock Heat Losses In' Thermal Reservoir Simulators. *Petroleum Society of Canada*. doi:10.2118/80-03-04

Wang, H., Sweatman, R. E., Engelman, R., Deeg, W. F. J., Whitfill, D. L., Soliman, M. Y., and Towler, B. F. 2008. Best Practice in Understanding and Managing Lost Circulation Challenges. *Society of Petroleum Engineers*. doi:10.2118/95895-PA.

Warpinski, N. R., and Teufel, L. W. 1987. Influence of Geologic Discontinuities on Hydraulic Fracture Propagation (includes associated papers 17011 and 17074). *Society of Petroleum Engineers*. doi:10.2118/13224-PA

Willis-Richards, J., Watanabe K., Takahashi H. 1996. Progress toward a stochastic rock mechanics model of engineered geothermal systems. *Journal of Geophysical Research 101* (B8): 17481-17496, doi: 10.1029/96JB00882.

Witherspoon, P. A., Wang J. S. Y., Iwai K., Gale J. E. 1980. Validity of cubic law for fluid flow in a deformable rock fracture. *Water Resources Research 16* (6): 1016-1024, doi: 10.1029/WR016i006p01016.

Zhou, J., Chen, M., Jin Y., and Zhang G.-q. 2008. Analysis of fracture propagation behavior and fracture geometry using a tri-axial fracturing system in naturally fractured reservoirs. *International Journal of Rock Mechanics and Mining Sciences*, 45(7), 1143-1152, doi:10.1016/j.ijrmms.2008.01.001.